

1 Authors' answers to **Anonymous Referee #3**

2  
3 The authors have made an effort to carefully address all the comments put forward by the reviewers and  
4 have improved the manuscript. In my opinion it is almost ready for publication, given some small  
5 amendments.

6 Dear reviewer, we thank you for reviewing our manuscript for the second time. You will find our  
7 answers in line with your comments below:

8  
9 (title)

10 I am not convinced by the new title of the manuscript. The „rollercoaster“ and the „swarm“ are not sufficiently  
11 self-explanatory acronyms to allow sense-making of the title. I strongly encourage finding a title that is catchy  
12 because it speaks for itself. Why not including the terms „variation“ and „rooting depth“ into the title?

13 We have changed the title to a version close to its original form, but integrating the important  
14 keywords suggested by the referee:

15 *“Disentangling temporal and population variability in plant root water uptake from stable*  
16 *isotopic analysis: when rooting depth matters in labeling studies”*

17  
18 (abstract)

19 The abstract still includes some sentences that are difficult to understand without having read the paper. I  
20 propose properly rephrasing. Specifically -

21 Line 32-33: „the variability captured by  $\delta_{\text{tiller}}$  was spatial and may not correlate with the temporal dynamics  
22 of  $\psi_{\text{leaf}}$ .”

23 We attempted to make our point clearer and edited the sentence as (now L32-35):

24 *“...the variability captured by  $\delta_{\text{tiller}}$  reflected the spatial heterogeneity in rooting depth in the*  
25 *soil region influenced by the labeling and may not correlate with the temporal dynamics of*  
26  *$\psi_{\text{leaf}}$ . In other words, the strong variations of RWU as deduced from isotopic changes in the*  
27 *tiller water may not translate into significant variations of leaf water potential value.”*

28  
29 Line 36-37: The reference to hydraulic lift comes a bit out of the blue. I expected the last sentence of the  
30 abstract to address further implications, but not a completely new topic. It is confusing. Can you  
31 accommodate this?

32 We now underline that the very last sentence in the abstract is not a new topic but illustrates another  
33 fundamental difference between the physical and statistical model (now L38-40):

34 *“An important difference between the two types of RWU models was the ability of the*  
35 *physical model to simulate the occurrence of hydraulic lift in order to explain concomitant*  
36 *increases of soil water content and isotopic composition observed overnight above the soil*  
37 *labeling region.”*

38  
39 (List of variables)

40  $Se_j$  is now added to list of variables. However, please adhere to the HESS guidelines which require variable  
41 abbreviations in equations to be one letter only. Therefore, the abbreviation  $Se$  should be changed.

42 Thank you. The symbol “ $Se$ ” is standard for soil relative water content in vadose zone hydrology,  
43 so we modified it into “ $Se_e$ ” with “ $e$ ” part of the subscript so that the main symbol “ $S$ ” is one letter as  
44 requested by HESS guidelines. We therefore adapted the text in section “2.4 Modeling of RWU and  
45  $\delta_{\text{tiller}}$ ” (now L206-211):

46 The soil hydraulic conductivity function of Mualem [1976] and van Genuchten [1980] was  
 47 used:

$$48 \quad k_{soil,j}(t) = k_{sat} \cdot S_{e,j}^{\lambda} \left(1 - \left(1 - S_{e,j}^{\frac{1}{m}}\right)^m\right)^2 \quad (4)$$

49 where (...)  $S_{e,j}$ , the relative water content (dimensionless), is computed from the saturated  
 50 ( $\theta_{sat}$ , m<sup>3</sup> m<sup>-3</sup>) and residual ( $\theta_{res}$ , m<sup>3</sup> m<sup>-3</sup>) water contents as:

$$51 \quad S_{e,j} = \frac{\theta_j - \theta_{res}}{\theta_{sat} - \theta_{res}} \quad (5)$$

52  
 53  
 54  
 55 (Methods)

56 Line 188: „the right amount of plants“ - do you mean „the right number of plants“ ? Also, it is unclear what is  
 57 meant with „right“. Could you please specify?

58 Thank you for spotting this point that requires clarification. In the revised version of the text, we  
 59 rephrased the sentence as follows (now L190-191):

60 “In order to reach a total number of virtual plants representative of the number of plants in the  
 61 experimental setup, each root system was replicated 5 times, forming a “group”.”

62  
 63 Line 222: In the response to the review 3 it says the new text would read “big leaf”, but in the new manuscript  
 64 version it only says „leaf“. The „big leaf“, as in the response to reviewer 3, would be better.

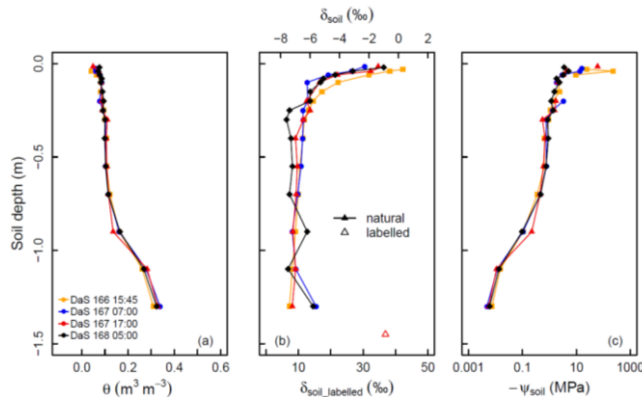
65 Thank you for noticing this oversight on our behalf. In the revised version of the text, we used the  
 66 term “big leaf” as in the reply to the referee (now L224-226):

67 “...  $K_{soil-root}$  represents the water flow per unit water potential difference between the SSF-averaged  
 68 bulk soil water potential and the “big leaf” (assuming a negligible stem hydraulic resistance [Steudle and  
 69 Peterson, 1998].”

70  
 71 Figure 2:

72 I think panel c would be much easier to read, if the x-axis was simply log-scale instead of plotting log(  
 73 \psi\_soil)

74 You are right! This is done. The new Figure 2 is displayed below:



75

76 **Disentangling temporal and population variability in plant root**  
77 **water uptake from stable isotopic analysis: when rooting depth**  
78 **matters in labeling studies**~~The rollercoaster and the swarm:~~  
79 **disentangling plant water isotopic composition variabilities in**  
80 **response to soil water labelling**

81 Valentin Couvreur<sup>1\*</sup>, Youri Rothfuss<sup>2\*</sup>, Félicien Meunier<sup>3</sup>, Thierry Bariac<sup>4</sup>, Philippe Biron<sup>4</sup>, Jean-  
82 Louis Durand<sup>5</sup>, Patricia Richard<sup>4</sup>, and Mathieu Javaux<sup>1,2</sup>

83 <sup>1</sup>Earth and Life Institute (ELI), Université catholique de Louvain (UCL), Louvain-la-Neuve, 1348, Belgium

84 <sup>2</sup>Institute of Bio- and Geosciences, IBG-3 Agrosphere, Forschungszentrum Jülich GmbH, Jülich, 52425, Germany

85 <sup>3</sup>CAVElab - Computational and Applied Vegetation Ecology, Faculty of Bioscience Engineering, Ghent University,  
86 Campus Coupure links 653, Gent, 9000, Belgium

87 <sup>4</sup>Institute of Ecology and Environmental Sciences (IEES) – Paris, UMR 7618, CNRS-Sorbonne Université, Campus  
88 AgroParisTech, Thiverval-Grignon, 78850, France

89 <sup>5</sup>UR P3F (INRA), Lusignan, 86600, France

90 *Correspondence to:* Valentin Couvreur ([valentin.couvreur@uclouvain.be](mailto:valentin.couvreur@uclouvain.be)) and Youri Rothfuss ([y.rothfuss@fz-](mailto:y.rothfuss@fz-)  
91 [juelich.de](mailto:y.rothfuss@fz-juelich.de))

92 \* These authors contributed equally to this work.

93 **Abstract.** Isotopic labeling techniques have the potential to minimize the uncertainty of plant root water uptake (RWU)  
94 profiles estimated through multi-source (statistical) modeling, by artificially enhancing soil water isotopic gradient.

95 On the other end of the modelling continuum, physical models can account for hydrodynamic constraints to RWU if  
96 simultaneous soil and plant water status data is available.

97 In this study, a population of tall fescue (*Festuca arundinaceae* cv Soni) was grown in a macro-rhizotron and monitored  
98 for a 34-hours long period following the oxygen stable isotopic (<sup>18</sup>O) labeling of deep soil water. Aboveground  
99 variables included tiller and leaf water oxygen isotopic compositions ( $\delta_{\text{tiller}}$  and  $\delta_{\text{leaf}}$ ) as well as leaf water potential  
100 ( $\psi_{\text{leaf}}$ ), relative humidity, and transpiration rate. Belowground profiles of root length density (RLD), soil water content  
101 and isotopic composition were also sampled. While there were strong correlations between hydraulic variables as well  
102 as between isotopic variables, the experimental results underlined the partial disconnection between temporal dynamics  
103 of hydraulic and isotopic variables.

104 In order to dissect the problem, we reproduced both types of observations with a one-dimensional physical model of  
 105 water flow in the soil-plant domain, for 60 different realistic RLD profiles. While simulated  $\psi_{\text{leaf}}$  followed clear  
 106 temporal variations with little differences across plants as if they were “on board of the same rollercoaster”, simulated  
 107  $\delta_{\text{tiller}}$  values within the plant population were rather heterogeneous (“swarm-like”) with relatively little temporal  
 108 variation and a strong sensitivity to rooting depth. The physical model thus explained the discrepancy between isotopic  
 109 and hydraulic observations: the variability captured by  $\delta_{\text{tiller}}$  reflected was the spatial heterogeneity in rooting depth in  
 110 the soil region influenced by the labeling and spatial and may not correlate with the temporal dynamics of  $\psi_{\text{leaf}}$ . In  
 111 other words, the strong variations of RWU as deduced from isotopic changes in the tiller water may not translate into  
 112 significant variations of leaf water potential value.  
 113 For comparison purposes, a Bayesian statistical model was also used to simulate RWU. While they predicted relatively  
 114 similar cumulative RWU profiles, the physical model could differentiate spatial from temporal dynamics of the isotopic  
 115 compositions signature. An important difference between the two types of RWU models was the ability of the physical  
 116 model to simulate the occurrence of hydraulic lift in order It further supported that to explain concomitant increases of  
 117 soil water content and isotopic composition observed overnight above the soil region influenced by the labeling  
 118 region were due to hydraulic lift.

#### 119 List of variables with symbols and units

120	Name	Symbol	Units
121	Leaf water potential/head:	$\psi_{\text{leaf}}$	MPa
122	Soil water potential/head:	$\psi_{\text{soil}}$	MPa
123	Water volumetric mass:	$\rho_w$	$\text{kg m}^{-3}$
124	Soil apparent density:	$\rho_b$	$\text{kg m}^{-3}$
125	Soil gravimetric water content:	$\theta_{\text{grav}}$	$\text{kg kg}^{-1}$
126	Soil volumetric water content:	$\theta$	$\text{m}^3 \text{m}^{-3}$
127	Intensity of water uptake (sink term):	$S$	$\text{d}^{-1}$
128	Transpiration rate per unit soil area:	$T$	$\text{m d}^{-1}$
129	Air relative humidity	RH	%
130	Soil horizontal area:	$A_{\text{soil}}$	$\text{m}^2$
131	Soil layer depth (for each layer):	$z$	m
132	Soil layer thickness (for each layer):	$\Delta Z$	m
133	Root length (for each soil layer):	$l_{\text{root}}$	m
134	Relative Root Water Uptake	rRWU	dimensionless
135	Best run	$br$	dimensionless
136	Root Length Density:	RLD	$\text{m m}^{-3}$
137	Soil water oxygen isotopic composition:	$\delta_{\text{soil}}$	‰
138	Tiller water oxygen isotopic composition:	$\delta_{\text{tiller}}$	‰
139	Leaf water oxygen isotopic composition:	$\delta_{\text{leaf}}$	‰
140	Soil-root system conductance:	$K_{\text{soil-root}}$	$\text{m}^3 \text{MPa}^{-1} \text{s}^{-1}$
141	Soil-root radial conductance:	$K_{\text{radial}}$	$\text{m}^3 \text{MPa}^{-1} \text{s}^{-1}$

142	Root radial conductivity:	$L_{pr}$	$m MPa^{-1} s^{-1}$
143	Root axial conductance:	$K_{axial}$	$m^3 MPa^{-1} s^{-1}$
144	Equivalent root axial conductivity:	$k_{axial}$	$m^4 MPa^{-1} s^{-1}$
145	Soil hydraulic conductivity:	$k_{soil}$	$m^2 MPa^{-1} s^{-1}$
146	Saturated soil hydraulic conductivity:	$k_{sat}$	$m^2 MPa^{-1} s^{-1}$
147	Soil hydraulic conductivity parameter	$\lambda$	dimensionless
148	Soil relative water content	$\theta_r$	dimensionless
149			

- Formatted: English (United States)
- Formatted: English (United States)
- Formatted: English (United States)
- Formatted: English (United States)
- Formatted: English (United States)

150 **1 Introduction**

151 Since the seminal work of Washburn and Smith [1934] where it was first reported that willow trees did not fractionate  
152 hydrogen stable isotopes in a hydroponic water solution during root water uptake (RWU), water stable isotopologues  
153 ( $^1\text{H}^2\text{H}^{16}\text{O}$  and  $^1\text{H}_2^{18}\text{O}$ ) have been used as indicators for plant water sources in soils. In their review, Rothfuss and  
154 Javaux [2017] reported in the period 2015-2016 about no less than 40 publications in which RWU was retrieved from  
155 stable isotopic measurements. Novel measuring techniques (e.g., cavity ring-down spectroscopy – CRDS and off-axis  
156 integrated cavity output spectroscopy – ICOS) providing ways for fast and cost-effective water stable isotopic analyses  
157 certainly enable and emulate current research in that field. Water stable isotopologues are no longer powerful tracers  
158 waiting for technological developments [Yakir and Sternberg, 2000] but are on the verge to be used to their full  
159 potential for addressing eco-hydrological research questions and identify processes in the soil-plant-atmosphere  
160 continuum [Werner et al., 2012; Dubbert and Werner, 2019; Sprenger et al., 2016].

161 The isotopic determination of RWU profiles is based on the principle that the isotopic composition of xylem water at  
162 the outlet of the root system (i.e., in the first aerial and non-transpiring node of the plant) equals the sum of the product  
163 between the soil water isotopic composition and relative contribution to RWU across plant water sources. Results come  
164 only with reasonable precision when (i) the soil water isotopic composition depth gradient is strong and monotonic  
165 (thus avoiding issues of identifiability) and (ii) the temporal dynamics of RWU and soil water isotopic composition is  
166 relatively low. Condition (i) is fulfilled mostly at the surface of the soil, while soil water isotopic composition gradients  
167 become usually lower or null with increasing depth (due to the isotopic influence of the groundwater table and  
168 increasing dispersion with depth). As illustrated by Oerter and Bowen [2019], the lateral variability of the soil water  
169 isotopic composition profiles can become significant in the field and could have great implications on the  
170 representability and meaningfulness of isotopic-derived estimate of RWU profiles. Condition (ii) is often neglected  
171 but is required due to the instantaneous nature of the sap flow samples.

172 To overcome these limitations, labeling pulses have been increasingly used in recent works to artificially alter the  
173 natural isotopic gradients [e.g., Beyer et al., 2016; Beyer et al., 2018; Grossiord et al., 2014; Jesch et al., 2018;  
174 Volkmann et al., 2016b]. However, a precise characterization of the artificial spatial (i.e., lateral and vertical) and  
175 temporal distributions of the soil water isotopic composition (driven by e.g., soil isotopic water flow) is crucial. The  
176 punctual assessments of the isotopic composition profiles following destructive sampling in the field and subsequent  
177 extraction of water in the laboratory might neither be spatially nor temporally representative and can lead to erroneous  
178 estimates of RWU profiles [Orlowski et al., 2018; Orlowski et al., 2016a].

179 The vast majority of isotopic studies use statistical (e.g., Bayesian) modeling to retrieve RWU profile solely from the  
180 isotopic composition of water extracted in the soil and the shoot [Rothfuss and Javaux, 2017]. However, when data on  
181 soil and plant water status is available, hydraulic modeling tools can also be used to connect different data types in a  
182 process-based manner and estimate root water uptake profiles [Passot et al., 2019]. Some of the most simplistic models

183 use 1-D relative root distribution and plant-scale hydraulic parameters [Sulis et al., 2019], while the most complex rely  
184 on root architectures and root segment permeabilities [Meunier et al., 2017c]. Only a handful of studies coupled  
185 isotopic measurements in plant tissues and soil material with models describing RWU in a mechanistic manner. For  
186 instance, Meunier et al. [2017a] could both locate and quantify the volume of redistributed water by *Lolium multiflorum*  
187 by labeling of the soil with  $^{18}\text{O}$  enriched water under controlled conditions.

188 Building on the work of Meunier et al. [2017a], the objective of the present study is to (i) model in a physically-based  
189 manner (i.e., by accounting for soil and plant and environmental factors) the temporal dynamics of the isotopic  
190 composition of RWU of a population of *Festuca arundinacae* cv Soni. (tall fescue) during a semi-controlled  
191 experiment following an isotopic labeling of deep soil water, (ii) investigate the implication of the model-to-data fit  
192 quality in terms of meaningfulness of the isotopic information to reconstruct RWU profiles, and finally (iii) confront  
193 the simulated root water uptake profiles with estimations obtained on basis of isotopic information alone (i.e., provided  
194 by a Bayesian mixing model).

## 195 **2 Material and methods**

196 Our experiment consisted in supplying labeled water from the bottom to a macro-rhizotron in which tall fescue was  
197 grown. Data on soil and plant oxygen stable isotopic [signature composition](#) and hydraulic status were monitored for  
198 34 hours. In the following, the oxygen isotopic composition of water will be expressed in per mil (‰) on the “delta”  
199 ( $\delta^{18}\text{O}$ ) scale with respect to the international water standard V-SMOW [Gonfiantini, 1978].

### 200 **2.1 Rhizotron experimental setup**

201 The macro-rhizotron (dimensions: 1.6 m x 1.0 m x 0.2 m, see picture in Appendix A) was placed inside a glasshouse  
202 (INRA Lusignan, France), where it was continuously weighed (KE1500, Mettler-Toledo, resolution: 20 g) to monitor  
203 water effluxes (i.e., bare soil evaporation or evapotranspiration). Underneath the soil compartment and in contact with  
204 it, a water reservoir (height: 0.1 m) filled with gravel acted as water table and allowed the supply of water to the  
205 rhizotron. The rhizotron was equipped with two sets of CS616 time domain reflectometer (TDR) profiles (Campbell  
206 Scientific, USA) with 30 cm long probe rods positioned at six depths (−0.05, −0.10, −0.30, −0.60, −1.05 and −1.30 m)  
207 and one profile of tensiometers (SMS 2000, SDEC-France) located at four depths (−0.05, −0.10, −0.30, and −0.60 m)  
208 in order to monitor the evolution of soil water volumetric content ( $\theta$ , in  $\text{m}^3 \text{m}^{-3}$ ) and matric potential ( $\psi_{\text{soil}}$ , in MPa).  
209 Finally, relative humidity (RH, %) was recorded above the vegetation with one humidity and temperature probe  
210 (HMP45D, Vaisala, Finland). The transparent polycarbonate sides (front and back) allowed the daily observations of  
211 root maximal depth. The experimental setup allowed precisely controlling the amount and  $\delta^{18}\text{O}$  of soil input water.

212 Another important feature was the soil depth (i.e., 1.60 m) which minimized the influence of the water table on  
213 superficial layers water content and  $\delta^{18}\text{O}$ .

## 214 **2.2 Soil properties and installation**

215 The soil substrate originates from the Lp horizon of an agricultural field part of the Observatory of Environment  
216 Research (ORE), INRA Lusignan, France (0°60W, 46°250N) which is classified as District Cambisol (particle size  
217 distribution: sand 15%, silt 65%, clay 20%). Prior installation in the rhizotron, the substrate was sieved at 2 mm and  
218 dried out in an air oven at 110 °C during 48 h to remove most of the residual water. 450 kg of soil was filled in the  
219 rhizotron by 0.10 m increment and compacted in order to reach a dry bulk density value of  $\rho_b = 1420 \text{ kg m}^{-3}$ . The  
220 closed-form soil water retention curve of van Genuchten [1980] was derived in a previous study by Meunier et al.  
221 [2017a] from synchronous measurements of soil water content and matric potential from saturated to residual water  
222 content (see Appendix B for its hydraulic parameters). It was used to compute the soil water matric potential ( $\psi_{\text{soil}}$ , in  
223 MPa) on basis of volumetric water content data during the present experiment.

## 224 **2.3 Experimental protocol**

225 After installation, the soil was gradually flooded with local water ( $\delta^{18}\text{O} = -6.8 \text{ ‰}$ ) from the bottom reservoir up to the  
226 top of the profile for a period of three days in order to reduce as much as possible the initial lateral and vertical  
227 heterogeneities in water content and  $\delta^{18}\text{O}$ . The tall fescue (*Festuca arundinaceae* cv Soni) was sown at a seeding  
228 density of  $3.6 \text{ g m}^{-2}$  (which corresponds for the rhizotron surface area of  $0.2 \text{ m}^2$  to roughly 300 plants) when soil water  
229 content reached  $0.25 \text{ m}^3 \text{ m}^{-3}$  (corresponding to pF 2.3) at  $-0.05 \text{ m}$ , as measured by the soil water sensors, and emerged  
230 12 days later. During a period of 165 day following seeding, the tall fescue cover was exclusively watered from the  
231 reservoir with local water in order to (i) keep the soil bottom layer ( $< -1.3 \text{ m}$ ) close to water saturation, and to (ii) not  
232 to disrupt the natural soil water  $\delta^{18}\text{O}$  profile.

233 166 days after seeding (DaS 166) the following conditions were fulfilled: (i) there was a strong soil water content  
234 gradient between the soil deep [ $-1.5 \text{ m}$ ,  $-1.0 \text{ m}$ ] and superficial [ $-0.3 \text{ m}$ ,  $0 \text{ m}$ ] layers, (ii) the tall fescue roots had  
235 reached a depth of  $-1.5 \text{ m}$  (observed through polycarbonate transparent sides). That same day at 17:00, the reservoir's  
236 water was labelled and its  $\delta^{18}\text{O}$  measured at  $+470 \text{ ‰}$ . Soil was sampled before (DaS 166 - 15:45) and after labeling on  
237 DaS 167 - 07:00, DaS 167 - 17:00 and DaS 168 - 05:00 using a 2 cm diameter auger through the transparent  
238 polycarbonate side of the rhizotron on four occasions from the surface down to  $-1.3 \text{ m}$  for the determination of soil  
239 gravimetric water content ( $\theta_{\text{grav}}$ , in  $\text{kg kg}^{-1}$ ) and oxygen stable isotopic composition ( $\delta_{\text{soil}}$ , in ‰). Gravimetric water  
240 content was then converted to volumetric water content ( $\theta = \theta_{\text{grav}} * \rho_b / \rho_w$ , in  $\text{m}^3 \text{ m}^{-3}$ , where  $\rho_b$  is the bulk soil density  
241 and  $\rho_w$  is the water density). The hypothesis of a constant value for  $\rho_b$  across the reconstructed soil profile was further



242 validated from the quality of the linear fit (coefficient of determination  $R^2 = 1.0$ ) between the  $\theta$  values measured by the  
243 sensors at the six available depths and ( $-0.05$ ,  $-0.10$ ,  $-0.30$ ,  $-0.60$ ,  $-1.05$  and  $-1.30$  m) and those computed from  $\theta_{grav}$ .  
244 On 40 occasions during a 34-hour long period three whole plants were sampled from the vegetation (i.e., 120 plants  
245 were sampled in total from the cover). Each plant's tiller and leaves were pooled into two separate vials. Dead material  
246 as well as the oldest living leaf around each tiller were removed in order not to contaminate tiller samples with  
247 transpiring material [Durand et al., 2007]. In addition, air water vapor was collected from the ambient atmosphere  
248 surrounding the rhizotron. The air was run at a flow rate of  $1.5 \text{ l min}^{-1}$  through two glass cold traps in series immersed  
249 in a mixture of dry ice and pure ethanol at  $-80^\circ\text{C}$ . Water from plant (i.e., tillers and leaves) and soil samples was  
250 extracted by vacuum distillation for 14 to 16 hours depending on the sample mass (e.g., ranging between 18 to 28 g  
251 for soil) at temperatures of  $60$  and  $90^\circ\text{C}$ , respectively. The residual water vapor pressure at the end of each successful  
252 extraction procedure invariably reached  $10^{-1}$  mbar. The oxygen isotopic compositions of tiller, leaf, and soil water  
253 (i.e.,  $\delta_{tiller}$ ,  $\delta_{leaf}$ , and  $\delta_{soil}$ ) together with that of atmospheric water vapor ( $\delta_{atm}$ ) were measured with an IRMS (Isoprep  
254 18 - Optima, Fison, Great-Britain, precision accuracy of  $0.15 \text{ ‰}$ ). Finally, leaf water potential ( $\psi_{leaf}$ , in MPa) was  
255 monitored with a pressure chamber on two leaves per sampled plant, and evapotranspiration rate (in  $\text{m d}^{-1}$ ) was derived  
256 from the changes in mass of the rhizotron at the same temporal scale as plant sampling.

257 Root biomass was determined from the horizontal sampling of soil between the polycarbonate sides using a 2 cm  
258 diameter auger at  $-0.02$ ,  $-0.08$ ,  $-0.10$ ,  $-0.40$ ,  $-0.55$ ,  $-0.70$ ,  $-0.90$ ,  $-1.10$ , and  $-1.30$  m soil depth. Each depth was  
259 sampled once to thrice. Each soil core was washed of soil particles and roots were collected over a 0.2 mm mesh filter,  
260 and dried at  $60^\circ\text{C}$  for 48 hours. Finally, Root Length Density (RLD, in  $\text{m root (m soil)}^{-3}$ ) distribution was determined  
261 from the root dry mass using the specific root length determined by Gonzalez-Dugo et al. [2005] specifically for tall  
262 fescue ( $95 \text{ m g}^{-1}$ ). The reader is referred to Appendix C for an overview of the type and timing of the different  
263 destructive measurements during the intensive sampling period.

#### 264 **2.4 Modeling of RWU and $\delta_{tiller}$**

265 The experimental setup included about 300 tall fescue plants. In order to limit the computational requirement in the  
266 inverse modelling loop, we only generated 60 virtual root systems whose rooting depths ranged from  $-1.30$  to  $-1.60$   
267 m depth [based on our own observations and those of the literature, e.g., Schulze et al., 1996; Fan et al., 2016] with  
268 the root architecture simulator CRootBox [Schnepf et al., 2018], so that the simulated RLD matched observations (Fig.  
269 1a). ~~In order to reach a total number of virtual plants representative of the number of plants in the experimental setup#4~~  
270 ~~order-to-reach-the-right-amount-of-plants~~, each root system was replicated 5 times, forming a “group”. Each group was  
271 assumed to occupy one sixtieth of the total horizontal area, and considered as a “big root” hydraulic network (5 identical  
272 plants per “big root”) with equivalent radial and axial hydraulic conductances (thus neglecting architectural aspects  
273 but accounting for each group's respective root length density profile).

274 The radial soil-root conductance between the bulk soil and each group's ( $i$ ) root surfaces in soil layer  $j$  ( $K_{radial,j}$ , m<sup>3</sup>  
 275 MPa<sup>-1</sup> d<sup>-1</sup>), as derived by Meunier et al. [2017a], was assumed as variable in time ( $t$ ):

$$276 \quad K_{radial,i,j}(t) = \frac{2\pi r_{root} l_{root,i,j} B_j L_{pr} k_{soil,j}(t)}{B_j k_{soil,j}(t) + r_{root} L_{pr}} \quad (1)$$

277 with  $r_{root}$  (m) the root radius,  $l_{root,i,j}$  (m) the root length of plants of group  $i$  in soil layer  $j$ ,  $L_{pr}$  (m MPa<sup>-1</sup> d<sup>-1</sup>) the root  
 278 radial hydraulic conductivity,  $k_{soil,j}$  (m<sup>2</sup> MPa<sup>-1</sup> d<sup>-1</sup>) the soil hydraulic conductivity in layer  $j$ , and  $B_j$  (dimensionless) a  
 279 geometrical factor simplifying the horizontal dimensions into radial domains between the bulk soil and root surfaces,  
 280 as given by Schroeder et al. [2009]:

$$281 \quad B_j = \frac{2(1-\rho_j)(1+\rho_j)}{z\rho_j^2 \ln \rho_j - \rho_j^2 + 1} \quad (2)$$

282 where  $\rho$  (dimensionless) represents the ratio of the distance between roots and the root averaged diameter. It can be  
 283 deduced from the observed root length density (RLD <sub>$j$</sub> , m m<sup>-3</sup>):

$$284 \quad \rho_j = \frac{\sqrt{\frac{1}{\pi RLD_j}}}{r_{root}} \quad (3)$$

285 The soil hydraulic conductivity function of Mualem [1976] and van Genuchten [1980] was used:

$$286 \quad k_{soil,j}(t) = k_{sat} \cdot S_{e,j}^\lambda \left(1 - \left(1 - S_{e,j}^{\frac{1}{m}}\right)^m\right)^2 \quad (4)$$

287 where  $k_{sat}$  (m<sup>2</sup> MPa<sup>-1</sup> d<sup>-1</sup>),  $m$  (dimensionless) and  $\lambda$  (dimensionless) are soil hydraulic parameters (with  $m = 1 - 2/n$ )  
 288 and  $S_{e,j} = \frac{S_{w,j} - S_{res,j}}{S_{sat,j} - S_{res,j}}$ , the relative water content (dimensionless), is computed from the saturated ( $\theta_{sat}$ , m<sup>3</sup> m<sup>-3</sup>) and residual ( $\theta_{res}$ ,  
 289 m<sup>3</sup> m<sup>-3</sup>) water contents as:

$$290 \quad S_{e,j} = \frac{\theta_j - \theta_{res}}{\theta_{sat} - \theta_{res}} \quad (5)$$

292 Unlike the geometrical parameter  $B$ , which defines a domain geometry between the bulk soil and roots of the overall  
 293 population, the  $l_{root}$  term is group specific ( $i$ ) and uses the simulated root length density profiles over an area  
 294 corresponding to one sixtieth of the total setup horizontal area:

$$295 \quad l_{root,i,j} = \frac{\Delta Z_j A_{soil} RLD_{i,j}}{60} \quad (6)$$

296 with  $\Delta Z$  (m) and  $A_{soil}$  (m<sup>2</sup>) the soil layer thickness and horizontal surface area, respectively.

297 To finalize the connection between root xylem and shoot, axial conductances per root system group ( $K_{axial}$ , m<sup>3</sup> MPa<sup>-1</sup>  
 298 d<sup>-1</sup>) were calculated as equivalent "big root" specific axial conductance per root system group ( $k_{axial}$ , m<sup>4</sup> MPa<sup>-1</sup> d<sup>-1</sup>, to  
 299 be optimized by inverse modelling) as:

$$300 \quad K_{axial,j} = \frac{k_{axial}}{\Delta Z_j} \quad (7)$$

301 At each time step, both the total soil-root system conductance ( $K_{soil-root}$ ,  $m^3 MPa^{-1} d^{-1}$ ) and the standard sink distribution  
302 ( $SSF$ , dimensionless, summing up to 1), were calculated from  $K_{radial}$  and  $K_{axial}$ , using the algorithm of Meunier et al.  
303 [2017b]. The variable  $SSF$  is the relative distribution of water uptake in each soil layer under vertically homogeneous  
304 soil water potential conditions [Couvreur et al., 2012], and  $K_{soil-root}$  represents the water flow per unit water potential  
305 difference between the  $SSF$ -averaged bulk soil water potential and the “big leaf” (assuming a negligible stem hydraulic  
306 resistance [Stedde and Peterson, 1998]).

307 Adding soil hydraulic conductance to the one-dimensional hydraulic model of Couvreur et al. [2014] yields the  
308 following solutions of leaf water potential ( $\psi_{leaf}$ , MPa) and water sink terms ( $S$ ,  $d^{-1}$ ) whose formulation approaches that  
309 of Nimah and Hanks [1973]:

$$310 \psi_{leaf}(t) = -\frac{T(t)}{K_{soil-root}(t)} + \sum SSF_j(t) \cdot \psi_{soil,j}(t) \quad (8)$$

311 Where one sixtieth of the overall transpiration rate ( $T$ ,  $m d^{-1}$ ) is allocated to each group, and  $\psi_{soil,j}$  (Mpa) is the soil  
312 water potential in soil layer  $j$ .

$$313 S_{i,j}(t) = \frac{K_{soil-root,i}(t) \cdot SSF_{i,j}(t) \cdot (\psi_{soil,j}(t) - \psi_{leaf,i}(t))}{A_{soil} \cdot \Delta Z_j} \quad (9)$$

314 where  $K_{soil-root}$  was assumed to control the compensatory RWU which arise from a heterogeneously distributed soil  
315 water potential, due to large axial conductances [Couvreur et al., 2012].

316 Finally, the tiller water oxygen isotopic composition ( $\delta_{tiller}$ ) was calculated as the average of local soil water oxygen  
317 isotopic compositions ( $\delta_{soil}$ ) weighted by the relative distribution of positive water uptakes (i.e., not accounting for  $\delta_{soil}$   
318 at locations where water is exuded by the root), assuming a perfect mixture of water inside the root system [Meunier  
319 et al., 2017a]:

$$320 \delta_{tiller} = \frac{\sum_{S_j > 0} S_j \cdot A_{soil} \cdot \Delta Z_j \cdot \delta_{soil}(t)}{\sum_{S_j > 0} S_j(t) \cdot A_{soil} \cdot \Delta Z_j} \quad (10)$$

321 Like in the experiment,  $\delta_{tiller}$  from three plants were randomly pooled at each observation time. A hundred pools of 3  
322 plants (possibly including several plants of the same group) were randomly selected in order to obtain the pooled  
323 simulated  $\delta_{tiller}$  by arithmetic averaging.

324 The unknown parameters of the soil-root hydraulic model, i.e., the root radial conductivity ( $L_{pr}$ ), the root axial  
325 conductance ( $k_{axial}$ ), the soil saturated hydraulic conductivity ( $k_{sat}$ ), and the soil tortuosity factor ( $\lambda$ ) were finally  
326 determined by inverse modeling. For details on the procedure, the reader is referred to Appendix D.

327 In order to evaluate the robustness of the hydraulic model predictions (parametrized solely based on the reproduction  
328 of shoot observations in the inverse modeling scheme) from independent perspectives, we also compared predictions  
329 and measurements over 4 quantitative “soil-root domain” criteria: (i) the depth at which the transition between  
330 nighttime water uptake and exudation ( $S_{i,j} < 0$ , i.e. release of water from root to soil) takes place, (ii) quantities of exuded

331 water and overnight increase of soil water content, (iii) the enrichment of labelled water at the depth where water  
332 content increase is observed overnight, and (iv) the order of magnitude of the optimal root radial conductivity value as  
333 compared to literature data in tall fescue.

334 Finally, and as a comparison point, the Bayesian inference statistical model SIAR [Parnell et al., 2013] was used to  
335 determine the profiles of water sink terms of ten identified potential water sources. These water sources were defined  
336 to originate from 10 distinct soil layers (0.00-0.03, 0.03-0.07, 0.07-0.15, 0.15-0.30, 0.30-0.60, 0.60-0.90, 0.90-1.20,  
337 1.20-1.32, 1.32-1.37, and 1.37-1.44 m) for which corresponding  $\delta_{\text{soil}}$  values were computed [Rothfuss and Javaux,  
338 2017]. SIAR solely bases its estimates from the comparison of  $\delta_{\text{iller}}$  observations to the isotopic compositions of the  
339 soil water sources ( $\delta_{\text{soil}}$ ). For this,  $\delta_{\text{iller}}$  measurements were pooled in twelve groups corresponding to different time  
340 periods, selected to best reflect the observed temporal dynamics of  $\delta_{\text{iller}}$ . The reader is here referred to Appendix E for  
341 details on the model parametrization and running procedure.

## 342 **3 Results and discussion**

### 343 **3.1 Experimental data**

#### 344 **3.1.1 Soil profiles**

345 Figure 2a and b show a very stable soil water content profile and a more variable  $\delta_{\text{soil}}$  profile from DaS 166 - 15:45 to  
346 DaS 168 - 05:00. Soil was dry at the surface ( $0.058 \text{ m}^3 \text{ m}^{-3} < \theta < 0.092 \text{ m}^3 \text{ m}^{-3}$  for layer 0.015 - 0.040 m) whereas  
347 closer to saturation at depth  $-1.30 \text{ m}$  ( $\theta = 0.34 \text{ m}^3 \text{ m}^{-3} \pm 0.012 \text{ m}^3 \text{ m}^{-3}$ , estimated  $\theta_{\text{sat}} = 0.40 \text{ m}^3 \text{ m}^{-3}$ , see Appendix A).  
348 According to the measured soil matric potentials (Fig. 2c), soil water was virtually unavailable ( $\leq -1.5 \text{ MPa}$ ) above  $-$   
349  $0.5 \text{ m}$  depth. Soil moisture remained unchanged in the top 25 cm during the sampling period ( $\theta = 0.08 \pm 0.00 \text{ m}^3 \text{ m}^{-3}$ )  
350 as well as at  $-1.30 \text{ m}$  from DaS 166 - 15:45 to DaS 168 - 05:00 ( $\theta = 0.33 \pm 0.01 \text{ m}^3 \text{ m}^{-3}$ ), showing that roots were  
351 predominantly extracting water from deep soil layers.

352 Water in the top soil layers ( $-0.040 \text{ m} < z < -0.015 \text{ m}$ ) was isotopically enriched ( $-3.2 \text{ ‰} < \delta_{\text{soil}} < 0.3 \text{ ‰}$ ) as opposed  
353 to the deepest layer ( $\delta_{\text{soil}} = -7.34 \text{ ‰} \pm 0.30 \text{ ‰}$  at  $-1.30 \text{ m}$ ). Following labeling of the reservoir water on DaS 166 -  
354 17:00,  $\delta_{\text{soil}}$  reached a value of  $36.9 \text{ ‰}$  at  $-1.50 \text{ m}$  on DaS 167 - 17:00. The development of the vegetation on DaS 166-  
355 168 (LAI = 5.6) and the observed surface  $\theta$  values lead us to assume that the rhizotron water losses were due to  
356 transpiration flux solely (i.e., evapotranspiration = transpiration). The soil water oxygen isotopic exponential-shaped  
357 profiles were the product of fractionating evaporation flux, and to a great extent when the soil was bare or when the  
358 tall fescue cover was not fully developed. The differences in soil water oxygen isotopic profile observed at the four  
359 different sampling dates were therefore either due to lateral heterogeneity (e.g., upper soil layers), to the soil capillary  
360 rise of labelled water from the reservoir (deep soil layers), or to the hydraulic redistribution of water through roots (to  
361 the condition that the isotopic composition of the redistributed water differs from that of the soil water at the release

362 location). We noted an isotopic enrichment of 1.0 ‰ of soil water observed on DaS 168 - 05:00 at -0.9 m with respect  
363 to the mean  $\delta_{\text{soil}}$  value across previous sampling dates. This could partly be due to, e.g., upward preferential flow of  
364 labelled water from the bottom soil layers and therefore be the sign of the lateral heterogeneity of the soil. Another  
365 reason for this would be hydraulic redistribution of labelled water by the roots. It was however not possible to evaluate  
366 the relative importance of these three processes (lateral heterogeneity, capillary rise/preferential flow, and hydraulic  
367 redistribution) in the setting of the soil water isotopic profile since the physically-based soil-root model presented in  
368 section 2.4 does not account for soil liquid and vapor flow. This was also not the primary intent of the present study.  
369 The observed RLD profile (Fig. 1a) showed a typical exponential shape, i.e., maximum at the surface ( $5.42 \pm 0.34 \text{ cm}$   
370  $\text{cm}^{-3}$ ) down to a minimum at -1.10 m ( $0.540 \pm 0.35 \text{ cm cm}^{-3}$ ), while it increased again from the latter depth up to a  
371 value of  $1.660 \text{ cm cm}^{-3}$  at -1.30 m. This significant trend was most probably a direct consequence of the high soil  
372 water content value in this deeper layer.

### 373 3.1.2 Plant water and isotopic temporal dynamics

374 The temporal variation of  $\delta_{\text{tiller}}$  (Fig. 3a) was found to be either (i) moderate during day and night, i.e., from DaS 167 -  
375 06:00 to 11:00 ( $\delta_{\text{tiller}} = -2.6 \pm 1.4 \text{ ‰}$ ) and from DaS 167 - 21:30 to DaS 168 - 00:00 ( $\delta_{\text{tiller}} = -2.7 \pm 0.4 \text{ ‰}$ ), or (ii) strong  
376 during the day, i.e., from DaS 167 - 11:00 to 18:00 (maximum value of 20.9 ‰ at DaS 167 - 12:40), or else (iii) strong  
377 during the night, i.e., from DaS 167 - 04:00 to 06:00 (max = 36.4 ‰ at DaS 167 - 05:15) and from DaS 168 - 00:00 to  
378 06:00 (max = 14.6 ‰ at 28:00, DaS 168). Note that transpiration (Fig. 3b) occurred also at night during the sampling  
379 period, due to relatively high temperature in the glasshouse leading to a value of atmospheric relative humidity smaller  
380 than 85%, Fig. 3b). From 12:00 to 14:00 and from 16:00 to 17:00 on DaS 167 (case (ii)) high values of leaf transpiration  
381 corresponded to high values of  $\delta_{\text{tiller}}$ .

### 382 3.1.3 Partial decorrelation between water and isotopic state variables

383 Figure 4 shows that variables describing plant water status, i.e.,  $T$  and RH (Fig. 4a) and  $T$  and  $\psi_{\text{leaf}}$  (Fig. 4b) were well  
384 correlated: coefficient of determination  $R^2$  was equal to 0.78 and 0.70 for the entire experimental duration, respectively.  
385 However, linear relationships between water status and isotopic variables were either nonexistent, e.g., between  $T$  and  
386  $\delta_{\text{tiller}}$  ( $R^2=0.01$ , Fig. 4c) and between  $\psi_{\text{leaf}}$  and  $\delta_{\text{tiller}}$  ( $R^2=0.00$ , Fig. 4h) or characterized by a low  $R^2$  and high p-value  
387 (e.g., between  $T$  and  $\delta_{\text{leaf}}$ ,  $R^2=0.43$ ,  $p>0.05$ , Fig. 4d). The partial temporal disconnection between  $\delta_{\text{leaf}}$  and  $T$  could not  
388 be attributed to problems of the isotopic methodology, during e.g., the vacuum distillation of the water from the plant  
389 tillers and leaves: water recovery rate was always greater than 99 % and Rayleigh distillation corrections [Dansgaard,  
390 1964; Galewsky et al., 2016] were applied to standardize the observed oxygen isotopic composition values to a 100 %  
391 water recovery (based on the comparison of sample weight loss during distillation and mass of collected distilled  
392 water). The evolution of  $\delta_{\text{leaf}}$  was strongly correlated with that of  $\delta_{\text{tiller}}$  during the day ( $R^2 = 0.90$ ) whereas non-correlated

393 during the night ( $R^2 = 0.00$ , Fig. 4j). These observed correlations are in agreement with the Craig and Gordon [1965]  
394 model revisited by Dongmann [1974] and later by ~~and~~ Farquhar et al. [2007; 2005]. The model, which is extensively  
395 used in the current literature [e.g., Dubbert et al., 2017] states that, at isotopic steady-state,  $\delta_{\text{leaf}}$  is a function of the  
396 input water oxygen isotopic composition ( $\delta_{\text{tiller}}$ ) among other variables, i.e., leaf temperature (not measured during the  
397 experiment), stomatal and boundary layer conductances, oxygen isotopic composition of atmospheric water vapor, and  
398 relative humidity.

399 It is generally difficult to observe a statistically significant  $\delta_{\text{leaf}}-\delta_{\text{tiller}}$  (Fig. 4j) relationship at this temporal scale under  
400 natural abundance conditions in the field since the soil water isotopic weak gradient translates into weaker  $\delta_{\text{tiller}}$   
401 temporal dynamics. The quality of linear fit between  $\delta_{\text{leaf}}$  and  $\delta_{\text{tiller}}$  data collected during the day ( $R^2=0.90$ ) was made  
402 possible in this specific experiment by the artificial isotopic labeling pulse that enhanced the soil water isotopic  
403 gradient, which in turn increased the range of variation of  $\delta_{\text{tiller}}$ , ultimately highlighting the  $\delta_{\text{leaf}}-\delta_{\text{tiller}}$  temporal  
404 correlation. Air relative humidity is a driving variable of  $\delta_{\text{leaf}}$  in the model of Dongmann [1974] via the competing  
405 terms  $(1-RH)\cdot\delta_{\text{tiller}}$  and  $RH\cdot\delta_{\text{atm}}$ , where  $\delta_{\text{atm}}$  is the atmospheric water vapor isotopic composition inside the glasshouse.  
406 An overall significant linear correlation was observed between RH and  $\delta_{\text{leaf}}$  during the experiment ( $R^2=0.57$ , Fig. 4g).

407 During the two night periods (i.e., from 04:00-06:00 and from 20:30-07:00), as relative humidity increased in the  
408 glasshouse ( $51\% < RH < 85\%$ , Fig. 3b), the influence of the isotopic labeling of the tiller water (due to the labeling  
409 of deep soil water) through term  $(1-RH)\cdot\delta_{\text{tiller}}$  decreased to the benefit of term  $RH\cdot\delta_{\text{atm}}$  (with  $\delta_{\text{atm}}$  values ranging from  
410  $-15.9$  to  $-10.7\text{‰}$ , mean  $= -13.1 \pm 1.6\text{‰}$ , data not shown). This was especially visible between 04:50 and 06:00 on DaS  
411 167 and between 01:00 to 06:00 on DaS 168, when  $\delta_{\text{tiller}}$  reached greater values than  $\delta_{\text{leaf}}$ .

412 From a different perspective, as three plant water samples were pooled to reach a workable volume for the isotopic  
413 analysis at each observation time without replicates, the isotopic signal fluctuations may reflect both its temporal  
414 dynamics and its variability within the plant population.

## 415 3.2 Simulations

### 416 3.2.1 Rooting depth and transpiration rate control $\delta_{\text{tiller}}$ and $\psi_{\text{leaf}}$ fluctuations, respectively

417 Despite the use of a global optimizer and 4 degrees of freedom ( $L_{\text{pr}}$ ,  $k_{\text{axial}}$ ,  $k_{\text{sat}}$ ,  $\lambda$ , see optimal values in Table 1)  
418 specifically aiming at matching the simulated and observed temporal dynamics of  $\delta_{\text{tiller}}$ , none of the 60 root system  
419 groups or average population could reproduce the measured fluctuations in time ( $R^2=0.00$ , Fig. 5a), regardless of the  
420 weight attributed to this criterion in the objective function. The predicted versus observed  $\delta_{\text{tiller}}$  distributions including  
421 all plant groups and observation times differed noticeably but not significantly ( $6.6 \pm 8.4\text{‰}$  and  $3.7 \pm 8.4\text{‰}$ ,  
422 respectively) when pooling 3 simulated  $\delta_{\text{tiller}}$  randomly at each observation time ( $P>0.01$  in 92 cases out of 100 repeated  
423 drawings), as in measurements. Besides, the simulated  $\psi_{\text{leaf}}$  fitted well the observations ( $R^2=0.67$ , overall distributions:  
424  $-0.175 \pm 0.053$  MPa and  $-0.177 \pm 0.053$  MPa, respectively, Fig. 5c). When analyzing the distributions of  $\psi_{\text{leaf}}$  and  $\delta_{\text{tiller}}$

425 per maximum root system depth (Fig. 5b and d), it appears that the  $\psi_{\text{leaf}}$  signal is not sensitive to the rooting depth (Fig.  
426 5d), while  $\delta_{\text{tiller}}$  is more sensitive to rooting depth than to the temporal evolution of the plant environment (Fig. 5b).  
427 This leaves us with two hypotheses. The “rollercoaster hypothesis”:  $\delta_{\text{tiller}}$  rapidly goes up and down with all  
428 individuals on board of the same car (i.e. little variability within the population, unlike predictions in Fig. 5a, but like  
429 the simulated  $\psi_{\text{leaf}}$  in Fig. 5c). If that is correct, the physical model lacks a process that would capture the observed  
430 temporal fluctuations of  $\delta_{\text{tiller}}$ . The “swarm pattern hypothesis”:  $\delta_{\text{tiller}}$  is rather stable in time but its values within the  
431 plant population are dispersed like in a flying swarm, so that  $\delta_{\text{tiller}}$  values sampled at different times fluctuate, not due  
432 to temporal dynamics but to the fact that different individuals are sampled (Fig. 5a).  
433 The model suggests that the tall fescue population  $\psi_{\text{leaf}}$  follows a “rollercoaster” dynamics driven by transpiration rate,  
434 while the population  $\delta_{\text{tiller}}$  follows a “swarm” pattern driven by the maximum rooting depth of the sampled plants. As  
435 no correlation could be expected between the drivers (the maximum rooting depth of the sample plants and canopy  
436 transpiration rate), our analysis explains the absence of correlation between  $\delta_{\text{tiller}}$  and  $\psi_{\text{leaf}}$  or transpiration rate.  
437 In future experiments and in the specific context of labeling pulses, sampling more plants at each observation time  
438 would help disentangle the spatial from temporal sources of variability of  $\psi_{\text{leaf}}$  and  $\delta_{\text{tiller}}$ . It would however be at the  
439 cost of the temporal resolution of observations, or would necessitate a larger setup with more plants in the case of  
440 controlled conditions experiments.

### 441 3.2.2 Independent observations support the validity of the hydraulic model predictions

442 In the last 12 hours of the experiment (DaS 167 – 17:00 to DaS 168 – 05:00), the measured soil water content increased  
443 by  $0.029 \text{ m}^3 \text{ m}^{-3}$  at  $-0.9 \text{ m}$  depth, which could be a sign of nighttime hydraulic redistribution. During the same period,  
444 the physical model predicted a cumulative water exudation sufficient to increase soil water content by  $0.003 \text{ m}^3 \text{ m}^{-3}$ ,  
445 as soil water potential was sufficiently low to generate reverse flow, but high enough not to disrupt the hydraulic  
446 continuity between soil and roots [Carminati and Vetterlein, 2013; Meunier et al., 2017a]. While this increase is smaller  
447 than the observed water content change, it is only a component in the soil water mass balance. Given the soil water  
448 potential vertical gradient, upward soil capillary water flow may have accounted for another part of the observed  
449 moisture change. Experimental observations also show that  $\delta_{\text{soil}}$  increased by  $1.0 \text{ ‰}$  at  $0.9 \text{ m}$  depth during that time ( $-$   
450  $6.2 \text{ ‰}$ , a value significantly higher than  $-7.1 \text{ ‰} \pm 0.1 \text{ ‰}$  at earlier times based on ANOVA analysis,  $P < 0.01$ ), while  
451 our simulations of hydraulic redistribution generated an increase of  $\delta_{\text{soil}}$  by  $0.34 \text{ ‰}$ . As soil capillary flow may not  
452 generate local maxima of  $\delta_{\text{soil}}$  (no enrichment observed at surrounding depths, see Fig. 2b), and soil evaporation is  
453 assumed negligible at that depth, it is likely that the observed local enrichment was entirely due to hydraulic  
454 redistribution, which would then be underestimated by a factor of about 3 in our simulations. Increasing water  
455 exudation by a factor 3 would imply a simulated water content change due to exudation of  $0.0090 \text{ m}^3 \text{ m}^{-3}$  absolute  
456 water content, which remains compatible with the experimental observation. Between  $-1.1 \text{ m}$  and  $-0.9 \text{ depths}$ , the

457 nighttime water flow pattern transitioned from exudation to uptake in both measurements and predictions. At -1.1 m,  
458 the model predicted a cumulative water uptake sufficient to decrease soil water content by  $0.0101 \text{ m}^3 \text{ m}^{-3}$ , as compared  
459 to the observed  $0.0141 \text{ m}^3 \text{ m}^{-3}$  total soil water content decrease. The remaining  $0.004 \text{ m}^3 \text{ m}^{-3}$  water content decrease  
460 may have contributed to the recharge to the soil layers above through capillary flow, which was not simulated.  
461 Therefore, all relevant measurements (local increase of soil water content, local enrichment of water isotopic  
462 [signature composition](#)) and simulation results ( $S < 0$ , i.e. local water release from roots) clearly converge to the  
463 conclusion that hydraulic lift occurred in the vicinity of -0.9 m depth in the early morning of DaS 168.  
464 As far as fitted parameter values are concerned,  $L_{pr}$  ( $2.3 \cdot 10^{-7} \text{ m MPa}^{-1} \text{ s}^{-1}$ ) was in the range found by Martre et al.  
465 [2001] in tall fescue ( $2.2 \cdot 10^{-7} \pm 0.1 \text{ m MPa}^{-1} \text{ s}^{-1}$ ) and falls in the range obtained by Meunier et al. [2017a] for another  
466 grass (*Lolium multiflorum* Lam.,  $6.8 \cdot 10^{-8}$  to  $6.8 \cdot 10^{-7} \text{ m MPa}^{-1} \text{ s}^{-1}$ ). Our  $k_{axial}$  value cannot be compared to values of  
467 axial root conductance from the literature as it transfers the water absorbed by roots in a single “big root” per group  
468 of 5 identical plants. The optimal value of  $k_{sat}$  was quite high (Table 1) but reportedly very correlated to  $\lambda$  (i.e. soil  
469 unsaturated hydraulic conductivity is proportional to  $k_{sat}$ , but also to  $S_e^2$  [van Genuchten, 1980]), so that the low value  
470 of the latter compensated the high value of the former, thus they should be considered as effective rather than physical  
471 parameters.

### 472 3.2.3 Other sources of variability and observational error

473 Our treatment of the soil medium in this experiment (sieving, irrigation from the bottom) makes it laterally more  
474 homogeneous than natural soils. This method allowed us to study specifically the impact of the vertical gradients of  
475  $\delta_{soil}$  on  $\delta_{tiller}$ . It also justified the use of a simplistic 1-D model adapted to the vertically resolved measurements. If  
476 lateral heterogeneity of soil water content remained and was accounted for, our predictions of root water uptake  
477 distribution,  $\delta_{tiller}$  and  $\psi_{leaf}$  would be altered. Observational errors in the gravimetric soil water content measurement  
478 (turned into soil water potential using the soil water retention curve) would as well alter these predictions. In order to  
479 quantify the sensitivity of our simulated results to such heterogeneity or observational error, we varied the soil water  
480 content input by  $\pm 0.02 \text{ m}^3 \text{ m}^{-3}$  at three critical depths (-0.9, -1.1 and -1.3 m, before interpolation), at the last  
481 observation time, during which measurements and simulations suggested that hydraulic lift occurred. Our results were  
482 mostly sensitive to soil water content alterations at -0.9 m, and barely differed in response to alterations at -1.1 and -  
483 1.3 m, though the conclusions were not affected qualitatively. No statistically significant difference between predicted  
484 and observed  $\delta_{tiller}$  distributions for the overall dataset could be found when pooling 3 simulated  $\delta_{tiller}$  randomly at each  
485 observation time (predicted and observed  $\delta_{tiller}$  distributions were closest to differ when soil water content was reduced  
486 by  $0.02 \text{ m}^3 \text{ m}^{-3}$  at 0.9 m depth;  $P > 0.01$  in 76 cases out of 100 repeated drawings). Measured and simulated  $\psi_{leaf}$  remained  
487 very correlated in all cases (from  $R^2 = 0.69$  to  $0.74$  when adding or removing  $0.02 \text{ m}^3 \text{ m}^{-3}$  at 0.9 m depth, respectively).  
488 Furthermore, when adding or removing  $0.02 \text{ m}^3 \text{ m}^{-3}$  at 0.9 m depth, cumulative water exudation at -0.9 m varied

Formatted: Subscript



489 between 0.0019 and 0.0035 m<sup>3</sup> m<sup>-3</sup>, uptake at -1.1 m varied between 0.0080 and 0.0108 m<sup>3</sup> m<sup>-3</sup>, and the simulated  
490 change of  $\delta_{\text{soil}}$  ranged between 0.28 and 0.40 ‰, respectively.

491 Lateral heterogeneity of soil water isotopic composition may as well occur at the microscopic scale. As water in  
492 micropores is less mobile than water in meso- and macropores [Alletto et al., 2006], it is likely that, in the lower half  
493 of the profile, the capillary rise of labelled water affected the [signature composition](#) of water in meso- and macropores  
494 more than in micropores. If roots have more access to meso- and macropore water, then the water absorbed by roots  
495 would be isotopically enriched, as compared to the “bulk soil water” characterized experimentally. The importance of  
496 this possible bias depends on soil texture and heterogeneity (e.g. existence of more isolated “pockets” of soil or compact  
497 clusters), as well as on the speed of water mixing between mobile and immobile water fractions [Gazis and Feng,  
498 2004]. Including this process in the modelling would necessitate sufficient observations to estimate the aforementioned  
499 properties, and ideally some quantification of the lateral heterogeneity of soil water isotopic composition at the micro-  
500 scale.

501 The lateral heterogeneity of soil hydraulic properties and root distribution may also have participated to the generation  
502 of lateral soil water potential heterogeneities, particularly in undisturbed soils. If one had access to data on lateral  
503 heterogeneity of soil properties and rooting density, it would be possible to simulate 3D soil-root water flow with a  
504 tool such as R-SWMS [Javaux et al., 2008], using a randomization technique for soil properties distribution as in  
505 Kuhlmann et al. [2012], in order to obtain estimations of the relative importance of this type of heterogeneity on  $\delta_{\text{tiller}}$   
506 and  $\psi_{\text{leaf}}$  variability.

507 Unlike the tiller water isotopic [signature composition](#), leaf water potential turned out to be very sensitive to transpiration  
508 rate in our simulations (see temporal fluctuations of grey lines in Figure 5 panel c) and not very sensitive to root  
509 distribution (see small variations of leaf water potential across individuals in Figure 5 panel d). This suggests that in  
510 this setup the hydraulic conductance of the soil-root system limited shoot water supply more than the distribution of  
511 roots, as in Sulis et al. [2019]. Simulated baseline (i.e. for uniform transpiration rates) leaf water potentials are shown  
512 as grey lines in Figure 5 panel c, and measured leaf water potentials as a green line in the same panel. The fact that  
513 they match well, despite the high sensitivity of leaf water potential to transpiration rate, reinforces the idea that  
514 transpiration rate was likely not spatially heterogeneous among the plant population. Therefore, the tiller water isotopic  
515 [compositions signature](#), whose sensitivity to transpiration rate is already very low, was likely not affected by  
516 transpiration rate heterogeneity.

### 517 3.2.4 Do root water uptake profiles predicted by hydraulic and Bayesian models differ?

518 The root water uptake dynamics predicted by the mechanistic model are shown in Fig. 6a. The overall pattern of  
519 peaking water uptake in the lower part of the profile during daytime matched that of the statistical model, and the  
520 correlation coefficient of both model predictions was relatively high ( $R^2=0.53$ ) in average over the simulation period,

521 see Figure 7). The main differences were the following: (i) in the upper soil layers where the soil water potential was  
522 lower  $-1.5$  MPa, the statistical model predicted water uptake, which is theoretically impossible given the leaf water  
523 potential above  $-0.4$  MPa [van Den Honert, 1948]; (ii) In the upper half of the profile, the physical model predicted  
524 exudation at a rate limited by the low hydraulic conductivity between root surface and bulk soil, with a peak at night,  
525 at  $-0.9$  m depth (quantitative analysis in previous section); (iii) Below  $-1.0$  m depth, the water uptake rate predicted  
526 by the statistical model steadily increased with depth while that of the physical model was more uniform, likely due to  
527 axial hydraulic limitation [e.g., Bouda et al., 2018] counteracting the increasing soil water potential with depth. Note  
528 that the outcome of the statistical model may significantly depend on the definition of the a priori relative RWU  
529 (rRWU) profile. In the present study, we set it to follow a “flat” uniform distribution (i.e.,  $rRWU_j = 1/10$ , see Appendix  
530 E), in other words, each layer was initially defined to contribute equally to RWU. To the contrary of other studies [e.g.,  
531 Mahindawansa et al., 2018], where the a priori rRWU profile was empirically constructed on basis of soil water  
532 content and root length density profiles, we decided not to further arbitrarily constrain the Bayesian model for the sake  
533 of comparison with the physically-based soil-root model.

### 534 3.3 Progresses and Challenges in soil water isotopic labeling for RWU determination

535 Often in the field, the vertical dynamics of both soil water oxygen and hydrogen isotopic compositions are not strong  
536 enough (or show convolutions leading to issues of identifiability) for partitioning RWU among different contributing  
537 soil water sources. As a consequence, we unfortunately cannot make use of the natural variability in isotopic  
538 abundances for deciphering soil-root transfer processes [Beyer et al., 2018; Burgess et al., 2000]. To address this  
539 limitation of the isotopic methodology, labeling pulses have been applied locally at different depths in the soil profile  
540 [e.g., Beyer et al., 2016] or at the soil upper/lower boundaries under both lab and field conditions by mimicking rain  
541 events [e.g., Piayda et al., 2017] and/or rise of the groundwater table [Meunier et al., 2017a; Kühnhammer et al., 2019].  
542 After labeling, we are faced with two problems: (i) the labeling pulse might enhance RWU at the labeling location if  
543 the volume of added water significantly changes the value of soil water content. It therefore poses the question of the  
544 meaningfulness of the derived RWU profiles, and this independently from the model used (i.e., physically-based soil-  
545 root model or statistical multi-source mixing model). In other words: are we observing a natural RWU behavior of the  
546 plant individual or population or are we seeing the influence of the labeling pulse? Certainly a way to move forward  
547 is environmental observatories such as ecotron and field lysimeters [e.g., Groh et al., 2018; Benettin et al., 2018] that  
548 provide means to better constrain hydraulic boundary conditions and reduced their isotopic heterogeneity. They allow  
549 for a mechanistic and holistic understanding of soil-root processes from stable isotopic analysis.  
550 Another topic of concern is (ii) the difficulty to properly observe in situ (1) the propagation of the labeling pulse in the  
551 soil after application and (2) the temporal dynamics of the plant RWU isotopic composition. Beyer and Dubbert [2019]  
552 presented a comprehensive review on recent isotopic techniques for non-destructive, online, and continuous

553 determination of soil and plant water isotopic compositions [e.g., Rothfuss et al., 2013; Quade et al., 2019; Volkmann  
554 et al., 2016a] as alternatives of the widely used combination of destructive sampling and offline isotopic analysis  
555 following cryogenic vacuum extraction [Orlowski et al., 2016b] or liquid-vapor direct equilibration [Wassenaar et al.,  
556 2008]. These techniques have the potential for a paradigm change in isotopic studies on RWU processes to the  
557 condition that, e.g., isotopic effects during sample collection are fully understood.  
558 The present study highlights the need not to “trust” our isotope data alone and always complement them by information  
559 on environmental factors as well as on soil and plant water status to go beyond the simple application of statistical  
560 models. This is especially the case in the framework of labeling studies where strong soil water isotopic gradients may  
561 induce strong dynamics of the RWU isotopic composition from a low variability of rooting depths.

#### 562 **4 Conclusion**

563 In the present study, light could be shed on RWU of *Festuca arundinacae* by specifically manipulating the lower  
564 boundary conditions for water content and oxygen isotopic composition. The new version of the one-dimensional  
565 model of Couvreur et al. (2014) implemented here accounted for both root and soil hydraulics in a population of “big”  
566 root systems of known root length density profile. This approach underlined the high sensitivity of  $\delta_{\text{filler}}$  to rooting  
567 depth and suggested that if  $\delta_{\text{filler}}$  is measured on a limited number of individuals, its variations in time may reflect the  
568 heterogeneity of rooting depth within the population, rather than temporal dynamics which was minor in our  
569 simulations. The model avoided the prediction of water uptake at locations where it was physically unavailable (e.g.,  
570 in the top half of the soil profile), by accounting for water potential differences observed between the leaves and the  
571 soil, and explained quantitatively the local isotopic enrichment of soil water as the occurrence of nighttime Hydraulic  
572 Lift at -0.9 m depth. On the other hand, the Bayesian statistical approach tested for comparison, which was driven by  
573 isotopic information solely, naturally translated the observed changes of  $\delta_{\text{filler}}$  into profound temporal dynamics of  
574 RWU, at the expense of eco-physiological consideration (e. g., temporal dynamics of leaf water potential and  
575 transpiration rate).

576 This case study highlights (i) the potential limitations of water isotopic labeling techniques for studying RWU: the soil  
577 water isotopic artificial gradients induced from water addition result in an improvement in RWU profiles determination  
578 to the condition that they are properly characterized spatially and temporally. As already pointed out in the review of  
579 Rothfuss and Javaux (2017), the study also (ii) underlines the interest of complementing in-situ isotopic observations  
580 in soil and plant water with information on soil water status and plant ecophysiology; it finally (iii) calls for the use of  
581 simple soil-root models (though requiring additional water status measurements and making more explicit assumptions  
582 on the description of the soil-plant system, as compared to the traditional Bayesian approach) for inverting isotopic  
583 data and gain insights into the RWU process.

584 **Acknowledgements**

585 The experiment was part of the ASCHYD (“Biogeochemical characterization of Hydraulic Lift”) project and supported  
586 by the French EC2CO/BIOHEFFECT program (CNRS – INSU, ANDRA, BRGM, CNES, IFREMER, IRSTEA, IRD,  
587 INRA and Météo France). During the preparation of this manuscript, V.C. was supported by the Belgian National Fund  
588 for Scientific Research (FNRS, FC 84104) the Interuniversity Attraction Poles Programme-Belgian Science Policy  
589 (grant IAP7/29), and the “Communauté française de Belgique-Actions de Recherches Concertées” (grant ARC16/21-  
590 075); FM was first funded by the BAEF and the WBI, then by the FWO as a junior postdoc and is thankful to these  
591 organizations for their support.

592 **Data sets**

593 Upon acceptance, all research data needed for creating plots will be available in reliable FAIR-aligned data repositories  
594 with assigned DOIs.

595 **Author contribution**

596 TB, JLD, and PB designed the experiments and TB, JLD, PB, and YR carried them out. VC, FM, and MJ developed  
597 the physically-based root water uptake model code and VC and FM performed the simulations. YR performed the  
598 statistical simulations. VC, YR, FM, and MJ prepared the manuscript with contributions from all co-authors.

599 **Competing interests**

600 The authors declare that they have no conflict of interest.

601

602

603 **References**

- 604 Alletto, L., Coquet, Y., Vachier, P., and Labat, C. (2006), Hydraulic Conductivity, Immobile Water Content, and  
605 Exchange Coefficient in Three Soil Profiles, *Soil Science Society of America Journal*, 70, 1272-1280,  
606 10.2136/sssaj2005.0291.
- 607 Benettin, P., Volkmann, T. H. M., von Freyberg, J., Frentress, J., Penna, D., Dawson, T. E., and Kirchner, J. (2018),  
608 Effects of climatic seasonality on the isotopic composition of evaporating soil waters, *Hydrol. Earth Syst. Sc.*,  
609 22, 2881-2890, 10.5194/hess-22-2881-2018.
- 610 Beyrer, M., Koeniger, P., Gaj, M., Hamutoko, J. T., Wanke, H., and Himmelsbach, T. (2016), A deuterium-based  
611 labeling technique for the investigation of rooting depths, water uptake dynamics and unsaturated zone water  
612 transport in semiarid environments, *J. Hydrol.*, 533, 627-643, 10.1016/j.jhydrol.2015.12.037.
- 613 Beyrer, M., Hamutoko, J. T., Wanke, H., Gaj, M., and Koeniger, P. (2018), Examination of deep root water uptake  
614 using anomalies of soil water stable isotopes, depth-controlled isotopic labeling and mixing models, *J.*  
615 *Hydrol.*, 566, 122-136, 10.1016/j.jhydrol.2018.08.060.
- 616 Beyrer, M., and Dubbert, M. (2019), X Water Worlds and how to investigate them: A review and future perspective on  
617 in situ measurements of water stable isotopes in soils and plants, *Hydrol. Earth Syst. Sci. Discuss.*, in review  
618 10.5194/hess-2019-600.
- 619 Bouda, M., Brodersen, C., and Saiers, J. (2018), Whole root system water conductance responds to both axial and  
620 radial traits and network topology over natural range of trait variation, *J. Theor. Biol.*, 456, 49-61,  
621 10.1016/j.jtbi.2018.07.033.
- 622 Burgess, S. S. O., Adams, M. A., Turner, N. C., and Ward, B. (2000), Characterisation of hydrogen isotope profiles in  
623 an agroforestry system: implications for tracing water sources of trees, *Agric. Water Manage.*, 45, 229-241,  
624 Doi 10.1016/S0378-3774(00)00105-0.
- 625 Carminati, A., and Vetterlein, D. (2013), Plasticity of rhizosphere hydraulic properties as a key for efficient utilization  
626 of scarce resources, *Ann. Bot.*, 112, 277-290, 10.1093/aob/mcs262.
- 627 Couvreur, V., Vanderborght, J., and Javaux, M. (2012), A simple three-dimensional macroscopic root water uptake  
628 model based on the hydraulic architecture approach, *Hydrol. Earth Syst. Sc.*, 16, 2957-2971, 10.5194/hess-  
629 16-2957-2012.
- 630 Couvreur, V., Vanderborght, J., Beff, L., and Javaux, M. (2014), Horizontal soil water potential heterogeneity:  
631 simplifying approaches for crop water dynamics models, *Hydrol. Earth Syst. Sc.*, 18, 1723-1743,  
632 10.5194/hess-18-1723-2014.
- 633 Craig, H., and Gordon, L. I.: Deuterium and oxygen 18 variations in the ocean and marine atmosphere, *Stable Isotopes*  
634 *in Oceanographic Studies and Paleotemperatures*, Spoleto, Italy, 1965, 9-130, 1965.
- 635 Dansgaard, W. (1964), Stable Isotopes in Precipitation, *Tellus*, 16, 436-468, 10.1111/j.2153-3490.1964.tb00181.x.
- 636 Dongmann, G. (1974), Contribution of Land Photosynthesis to Stationary Enrichment of O-18 in Atmosphere, *Radiat.*  
637 *Environ. Biophys.*, 11, 219-225, 10.1007/Bf01323191.
- 638 Dubbert, M., Kübert, A., and Werner, C. (2017), Impact of Leaf Traits on Temporal Dynamics of Transpired Oxygen  
639 Isotope Signatures and Its Impact on Atmospheric Vapor, *Frontiers in Plant Science*, 8, 5,  
640 10.3389/fpls.2017.00005.
- 641 Dubbert, M., and Werner, C. (2019), Water fluxes mediated by vegetation: emerging isotopic insights at the soil and  
642 atmosphere interfaces, *New Phytol.*, 221, 1754-1763, 10.1111/nph.15547.
- 643 Durand, J. L., Bariac, T., Ghesquière, M., Biron, P., Richard, P., Humphreys, M., and Zwierzykowski, Z. (2007),  
644 Ranking of the depth of water extraction by individual grass plants using natural 18O isotope abundance,  
645 *Environ. Exp. Bot.*, 60, 137-144.
- 646 Fan, J. L., McConkey, B., Wang, H., and Janzen, H. (2016), Root distribution by depth for temperate agricultural crops,  
647 *Field Crops Res.*, 189, 68-74, 10.1016/j.fcr.2016.02.013.
- 648 [Farquhar, G. D., and Cernusak, L. A. \(2005\), On the isotopic composition of leaf water in the non-steady state, \*Funct. Plant Biol.\*, 32, 293-303, 10.1071/Fp04232.](#)
- 649

650 [Farquhar, G. D., Cernusak, L. A., and Barnes, B. \(2007\). Heavy water fractionation during transpiration. \*Plant Physiol.\*,](#)  
651 [143, 11-18, 10.1104/pp.106.093278.](#)

652 Galewsky, J., Steen-Larsen, H. C., Field, R. D., Worden, J., Risi, C., and Schneider, M. (2016), Stable isotopes in  
653 atmospheric water vapor and applications to the hydrologic cycle, *Rev. Geophys.*, 54, 809-865,  
654 10.1002/2015rg000512.

655 Gaziz, C., and Feng, X. (2004), A stable isotope study of soil water: evidence for mixing and preferential flow paths,  
656 *Geoderma*, 119, 97-111, [https://doi.org/10.1016/S0016-7061\(03\)00243-X](https://doi.org/10.1016/S0016-7061(03)00243-X).

657 Gonfiantini, R. (1978), Standards for stable isotope measurements in natural compounds, *Nature*, 271, 534-536,  
658 10.1038/271534a0.

659 Gonzalez-Dugo, V., Durand, J. L., Gastal, F., and Picon-Cochard, C. (2005), Short-term response of the nitrogen  
660 nutrition status of tall fescue and Italian ryegrass swards under water deficit, *Aust. J. Agric. Res.*, 56, 1269-  
661 1276, 10.1071/Ar05064.

662 Groh, J., Stumpp, C., Lucke, A., Putz, T., Vanderborght, J., and Vereecken, H. (2018), Inverse Estimation of Soil  
663 Hydraulic and Transport Parameters of Layered Soils from Water Stable Isotope and Lysimeter Data, *Vadose*  
664 *Zone J.*, 17, UNSP 170168  
665 10.2136/vzj2017.09.0168.

666 Grossiord, C., Gessler, A., Granier, A., Berger, S., Brechet, C., Hentschel, R., Hommel, R., Scherer-Lorenzen, M., and  
667 Bonal, D. (2014), Impact of interspecific interactions on the soil water uptake depth in a young temperate  
668 mixed species plantation, *J. Hydrol.*, 519, 3511-3519, 10.1016/j.jhydrol.2014.11.011.

669 Javaux, M., Schroder, T., Vanderborght, J., and Vereecken, H. (2008), Use of a three-dimensional detailed modeling  
670 approach for predicting root water uptake, *Vadose Zone J.*, 7, 1079-1088.

671 Jesch, A., Barry, K. E., Ravenek, J. M., Bachmann, D., Strecker, T., Weigelt, A., Buchmann, N., de Kroon, H., Gessler,  
672 A., Mommer, L., Roscher, C., and Scherer-Lorenzen, M. (2018), Belowground resource partitioning alone  
673 cannot explain the biodiversity–ecosystem function relationship: A field test using multiple tracers, *J. Ecol.*,  
674 106, 2002–2018., 10.1111/1365-2745.12947.

675 Kuhlmann, A., Neuweiler, I., van der Zee, S. E. A. T. M., and Helmig, R. (2012), Influence of soil structure and root  
676 water uptake strategy on unsaturated flow in heterogeneous media, *Water Resour. Res.*, 48,  
677 10.1029/2011wr010651.

678 [Kühnhammer, K., Kübert, A., Brüggemann, N., Deseano Diaz, P., van Dusschoten, D., Javaux, M., Merz, S.,](#)  
679 [Vereecken, H., Dubbert, M., and Rothfuss, Y. \(2019\). Investigating the root plasticity response of \*Centaurea\*](#)  
680 [jacea to soil water availability changes from isotopic analysis. \*New Phytol.\*, 226, 98-110,](#)  
681 [10.1111/nph.16352](#)~~Kühnhammer, K., et al. (2019). Investigating the root plasticity response of *Centaurea*~~  
682 ~~jacea to soil water availability changes from isotopic analysis." *New Phytologist*. 10.1111/nph.16352~~

683 Mahindawansa, A., Orłowski, N., Kraft, P., Rothfuss, Y., Racela, H., and Breuer, L. (2018), Quantification of plant  
684 water uptake by water stable isotopes in rice paddy systems, *Plant Soil*, 10.1007/s11104-018-3693-7.

685 Martre, P., Cochard, H., and Durand, J.-L. (2001), Hydraulic architecture and water flow in growing grass tillers  
686 (*Festuca arundinacea* Schreb.), *Plant Cell Environ*, 24, 65-76, 10.1046/j.1365-3040.2001.00657.x.

687 Meunier, F., Rothfuss, Y., Bariac, T., Biron, P., Durand, J.-L., Richard, P., Couvreur, V., J. V., and Javaux, M. (2017a),  
688 Measuring and modeling Hydraulic Lift of *Lolium multiflorum* using stable water isotopes, *Vadose Zone J.*,  
689 10.2136/vzj2016.12.0134.

690 Meunier, F., Couvreur, V., Draye, X., Vanderborght, J., and Javaux, M. (2017b), Towards quantitative root hydraulic  
691 phenotyping: novel mathematical functions to calculate plant-scale hydraulic parameters from root system  
692 functional and structural traits, *J. Math. Biol.*, 75, 1133-1170, 10.1007/s00285-017-1111-z.

693 Meunier, F., Draye, X., Vanderborght, J., Javaux, M., and Couvreur, V. (2017c), A hybrid analytical-numerical method  
694 for solving water flow equations in root hydraulic architectures, *Appl. Math. Model.*, 52, 648-663,  
695 10.1016/j.apm.2017.08.011.

696 Mualem, Y. (1976), A new model predicting the hydraulic conductivity of unsaturated porous media, *Water Resour.*  
697 *Res.*, 12, 513-522, 10.1029/WR012i003p00513.

Formatted: English (United States)

Formatted: English (United States)

698 Nimah, M. N., and Hanks, R. J. (1973), Model for Estimating Soil-Water, Plant, and Atmospheric Interrelations. I.  
699 Description and Sensitivity, *Soil Sci. Soc. Am. J.*, 37, 522-527, 10.2136/sssaj1973.03615995003700040018x.

700 Oerter, E., and Bowen, G. (2019), Spatio-temporal heterogeneity in soil water stable isotopic composition and its  
701 ecohydrologic implications in semiarid ecosystems, *Hydrol. Process.*, 33, 1724–1738, 10.1002/hyp.13434.

702 Orłowski, N., Breuer, L., and McDonnell, J. J. (2016a), Critical issues with cryogenic extraction of soil water for stable  
703 isotope analysis, *Ecohydrology*, 9, 3-10, 10.1002/eco.1722.

704 Orłowski, N., Pratt, D. L., and McDonnell, J. J. (2016b), Intercomparison of soil pore water extraction methods for  
705 stable isotope analysis, *Hydrol. Process.*, 30, 3434-3449, 10.1002/hyp.10870.

706 Orłowski, N., Breuer, L., Angeli, N., Boeckx, P., Brumbt, C., Cook, C. S., Dubbert, M., Dyckmans, J., Gallagher, B.,  
707 Gralher, B., Herbstritt, B., Herve-Fernandez, P., Hissler, C., Koeniger, P., Legout, A., Macdonald, C. J.,  
708 Oyarzun, C., Redelstein, R., Seidler, C., Siegwolf, R., Stumpp, C., Thomsen, S., Weiler, M., Werner, C., and  
709 McDonnell, J. J. (2018), Inter-laboratory comparison of cryogenic water extraction systems for stable isotope  
710 analysis of soil water, *Hydrol. Earth Syst. Sc.*, 22, 3619-3637, 10.5194/hess-22-3619-2018.

711 Parnell, A. C., Phillips, D. L., Bearhop, S., Semmens, B. X., Ward, E. J., Moore, J. W., Jackson, A. L., Grey, J., Kelly,  
712 D. J., and Inger, R. (2013), Bayesian stable isotope mixing models, *Environmetrics*, 24, 387–399,  
713 10.1002/env.2221.

714 Passot, S., Couvreur, V., Meunier, F., Draye, X., Javaux, M., Leitner, D., Pages, L., Schnepf, A., Vanderborght, J., and  
715 Lobet, G. (2019), Connecting the dots between computational tools to analyse soil-root water relations, *J.  
716 Exp. Bot.*, 70, 2345-2357, 10.1093/jxb/ery361.

717 Piayda, A., Dubbert, M., Siegwolf, R., Cuntz, M., and Werner, C. (2017), Quantification of dynamic soil-vegetation  
718 feedbacks following an isotopically labelled precipitation pulse, *Biogeosciences*, 14, 2293-2306, 10.5194/bg-  
719 14-2293-2017.

720 Quade, M., Klosterhalfen, A., Graf, A., Brüggemann, N., Hermes, N., Vereecken, H., and Rothfuss, Y. (2019), In-situ  
721 Monitoring of Soil Water Isotopic Composition for Partitioning of Evapotranspiration During One Growing  
722 Season of Sugar Beet (*Beta vulgaris*), *Agr. Forest Meteorol.*, 266–267, 53–64,  
723 10.1016/j.agrformet.2018.12.002.

724 Rothfuss, Y., Vereecken, H., and Brüggemann, N. (2013), Monitoring water stable isotopic composition in soils using  
725 gas-permeable tubing and infrared laser absorption spectroscopy, *Water Resour. Res.*, 49, 1-9,  
726 10.1002/wrcr.20311.

727 Rothfuss, Y., and Javaux, M. (2017), Reviews and syntheses: Isotopic approaches to quantify root water uptake: a  
728 review and comparison of methods, *Biogeosciences*, 14, 2199-2224, 10.5194/bg-14-2199-2017.

729 Schnepf, A., Leitner, D., Landl, M., Lobet, G., Mai, T. H., Morandage, S., Sheng, C., Zorner, M., Vanderborght, J.,  
730 and Vereecken, H. (2018), CRootBox: a structural-functional modelling framework for root systems, *Ann.  
731 Bot.*, 121, 1033-1053, 10.1093/aob/mcx221.

732 Schroeder, T., Javaux, M., Vanderborght, J., Korfgan, B., and Vereecken, H. (2009), Implementation of a Microscopic  
733 Soil-Root Hydraulic Conductivity Drop Function in a Three-Dimensional Soil-Root Architecture Water  
734 Transfer Model, *Vadose Zone J.*, 8, 783-792, 10.2136/vzj2008.0116.

735 Schulze, E. D., Mooney, H. A., Sala, O. E., Jobbagy, E., Buchmann, N., Bauer, G., Canadell, J., Jackson, R. B., Loreti,  
736 J., Oesterheld, M., and Ehleringer, J. R. (1996), Rooting depth, water availability, and vegetation cover along  
737 an aridity gradient in Patagonia, *Oecologia*, 108, 503-511, 10.1007/Bf00333727.

738 Sprenger, M., Leistert, H., Gimbel, K., and Weiler, M. (2016), Illuminating hydrological processes at the soil-  
739 vegetation-atmosphere interface with water stable isotopes, *Review of Geophysics*, 54, 674-704,  
740 10.1002/2015RG000515.

741 Steudle, E., and Peterson, C. A. (1998), How does water get through roots?, *J. Exp. Bot.*, 49, 775-788.

742 Sulis, M., Couvreur, V., Keune, J., Cai, G. C., Trebs, I., Junk, J., Shrestha, P., Simmer, C., Kollet, S. J., Vereecken,  
743 H., and Vanderborght, J. (2019), Incorporating a root water uptake model based on the hydraulic architecture  
744 approach in terrestrial systems simulations, *Agricultural and Forest Meteorology*, 269, 28-45,  
745 10.1016/j.agrformet.2019.01.034.

746 van Den Honert, T. H. (1948), Water transport in plants as a catenary process, *Discuss. Faraday Soc.*, 3, 146-153,  
747 10.1039/DF9480300146.  
748 van Genuchten, M. T. (1980), A closed-form equation for predicting the hydraulic conductivity of unsaturated soils,  
749 *Soil Sci. Soc. Am. J.*, 44, 892-898, 10.2136/sssaj1980.03615995004400050002x.  
750 Volkmann, T. H., Kühnhammer, K., Herbstritt, B., Gessler, A., and Weiler, M. (2016a), A method for in situ  
751 monitoring of the isotope composition of tree xylem water using laser spectroscopy, *Plant Cell Environ.*,  
752 10.1111/pce.12725.  
753 Volkmann, T. H. M., Haberer, K., Gessler, A., and Weiler, M. (2016b), High-resolution isotope measurements resolve  
754 rapid ecohydrological dynamics at the soil–plant interface, *New Phytol.*, 10.1111/nph.13868.  
755 Washburn, E. W., and Smith, E. R. (1934), The isotopic fractionation of water by physiological processes, *Science*,  
756 79, 188-189, 10.1126/science.79.2043.188.  
757 Wassenaar, L. I., Hendry, M. J., Chostner, V. L., and Lis, G. P. (2008), High resolution pore water  $\delta^2\text{H}$  and  
758  $\delta^{18}\text{O}$  measurements by  $\text{H}_2\text{O}(\text{liquid})\text{-H}_2\text{O}(\text{vapor})$  equilibration laser spectroscopy, *Environ. Sci.*  
759 *Technol.*, 42, 9262-9267.  
760 Werner, C., Schnyder, H., Cuntz, M., Keitel, C., Zeeman, M. J., Dawson, T. E., Badeck, F. W., Brugnoli, E.,  
761 Ghashghaie, J., Grams, T. E. E., Kayler, Z. E., Lakatos, M., Lee, X., Maguas, C., Ogee, J., Rascher, K. G.,  
762 Siegwolf, R. T. W., Unger, S., Welker, J., Wingate, L., and Gessler, A. (2012), Progress and challenges in  
763 using stable isotopes to trace plant carbon and water relations across scales, *Biogeosciences*, 9, 3083-3111,  
764 10.5194/bg-9-3083-2012.  
765 Yakir, D., and Sternberg, L. D. L. (2000), The use of stable isotopes to study ecosystem gas exchange, *Oecologia*, 123,  
766 297-311, 10.1007/s004420051016.



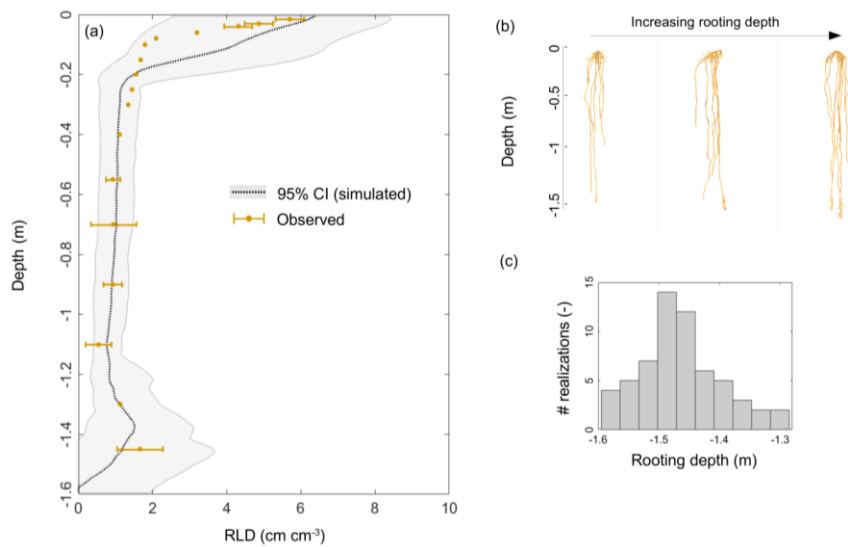
767 **5 Tables**

	$L_{pr}$ (m MPa <sup>-1</sup> s <sup>-1</sup> )	$k_{axial}$ (m <sup>4</sup> MPa <sup>-1</sup> s <sup>-1</sup> )	$k_{sat}$ (m <sup>2</sup> MPa <sup>-1</sup> s <sup>-1</sup> )	$\lambda$ (-)
Lower limit	10 <sup>-11</sup>	10 <sup>-13</sup>	10 <sup>-5</sup>	-5
Upper limit	10 <sup>-6</sup>	10 <sup>-8</sup>	10 <sup>-2</sup>	2
Value at best fit	2.3 10 <sup>-7</sup>	4.5 10 <sup>-11</sup>	9.5 10 <sup>-3</sup>	-4.9

768 **Table 1. Optimum and limits of the four-dimensional parametric space explored by the global optimization algorithm aiming**  
769 **at minimizing the difference between simulated and observed  $\delta_{filler}$  and  $\psi_{leaf}$ , as well as their standard deviation from average**  
770 **values during the full experiment.**

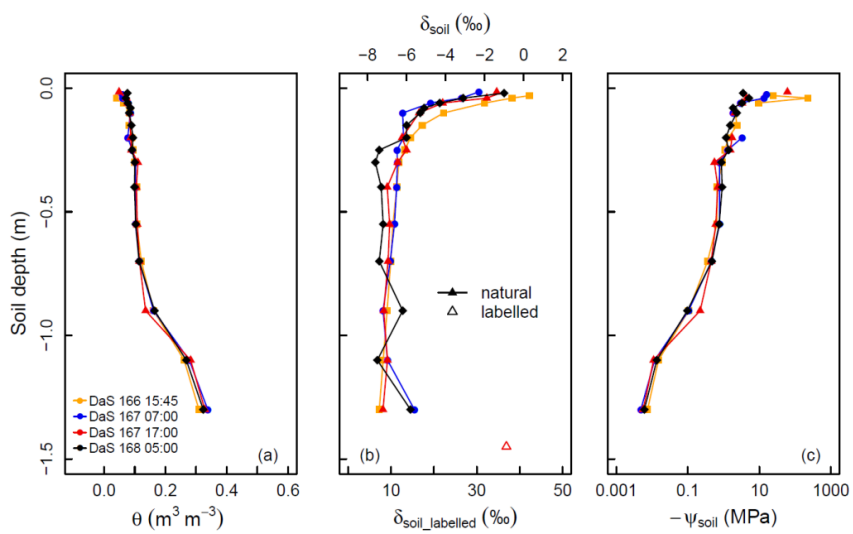
771 6 Figures

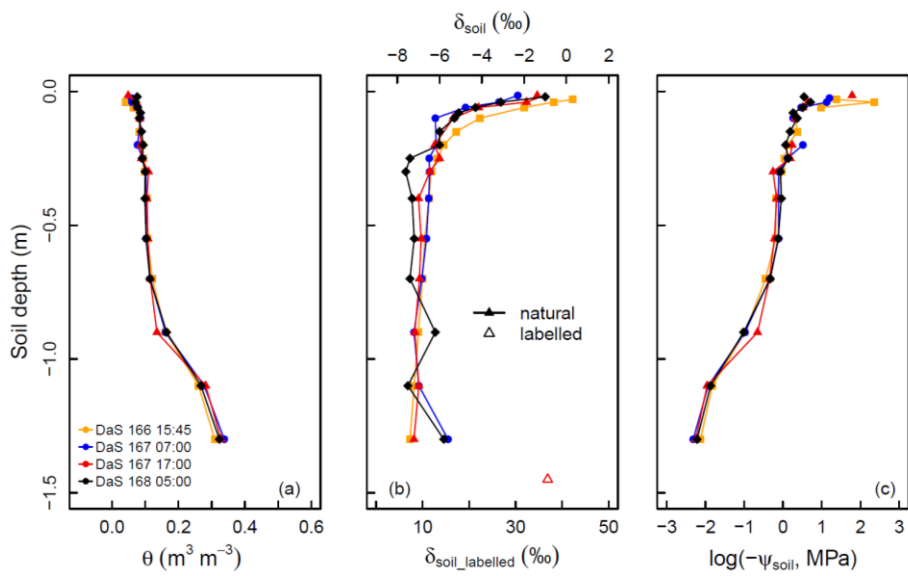
772



773

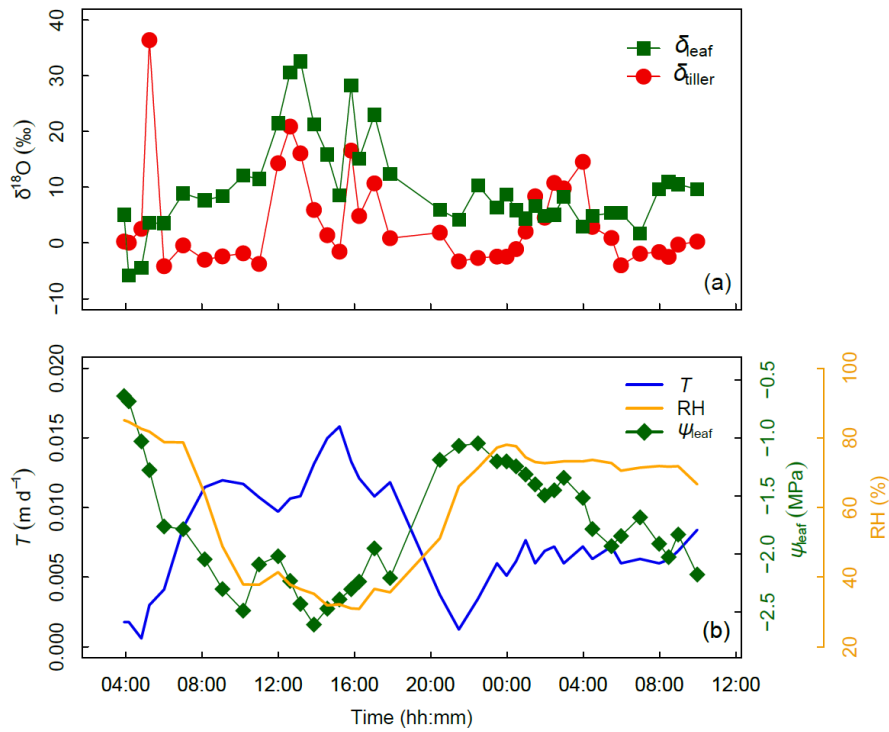
774 **Figure 1.** (a) Simulated (grey envelopes) and observed (brown dots) root length density profiles. Panels (b) and (c) illustrate  
775 the variability in modelled root system architectures and rooting depths, respectively.





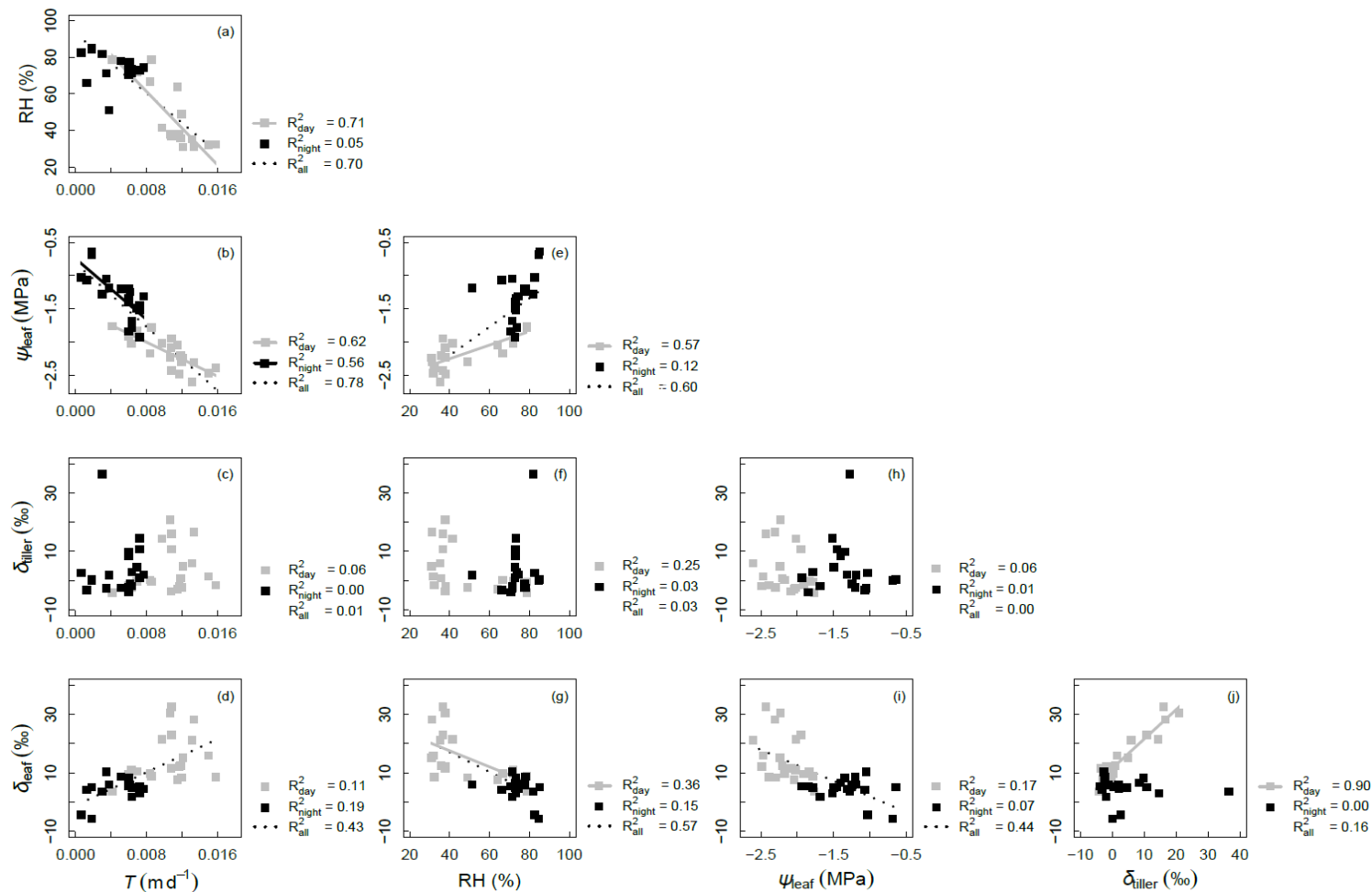
777  
778  
779

Figure 2. Measured soil volumetric water content ( $\theta$ , panel a), oxygen isotopic composition ( $\delta_{\text{soil}}$ , panel b), and calculated soil matric potential ( $\psi_{\text{soil}}$ , panel c) profiles during the sampling period.



780

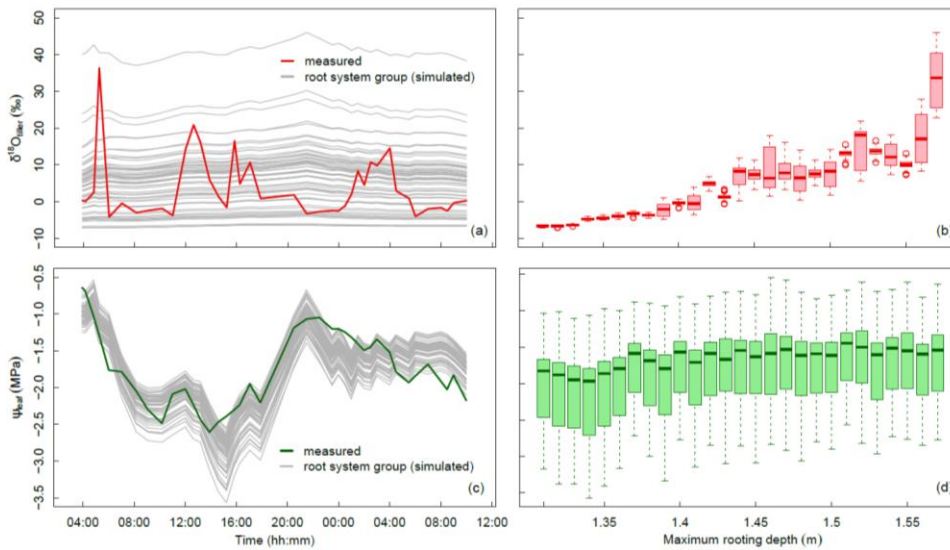
781 **Figure 3. (a) Time series of tiller and leaf water oxygen isotopic compositions ( $\delta_{\text{tiller}}$  and  $\delta_{\text{soil}}$ , ‰). (b) Transpiration flux ( $T$ ,  
 782 in  $\text{m d}^{-1}$ ), relative humidity (RH, %), and leaf water potential ( $\psi_{\text{leaf}}$ , in MPa, panel b) from days after seeding DaS 167 –  
 783 04:00 to DaS 168 – 11:00. Time of Labeling was DaS 166 – 17:00.**



784

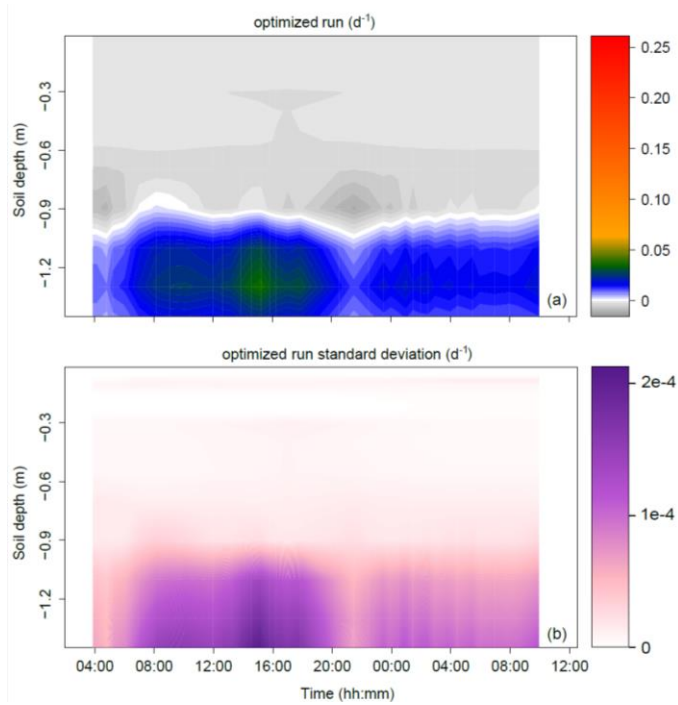
785 **Figure 4. Correlations between measured variables: oxygen isotopic compositions of xylem and leaf waters ( $\delta_{\text{tiller}}$  and  $\delta_{\text{leaf}}$ ,**  
 786 **in ‰), transpiration rate ( $T$ , in  $\text{m d}^{-1}$ ), relative humidity (RH, %), and leaf water potential ( $\psi_{\text{leaf}}$ , in MPa). Coefficient of**  
 787 **determinations ( $R^2$ ) are reported for all data, and separately for ‘day’ data (gray symbols) and ‘night’ data (black symbols)**  
 788 **(see Appendix C for definition of ‘day’ and ‘night’ experimental periods). Regression lines are drawn for linear models with**  
 789 **p-value < 0.01**

790



791

792 **Figure 5. Variation of  $\delta_{\text{diluter}}$  and  $\psi_{\text{leaf}}$  in time and across the 60 groups of simulated root systems. (a) Temporal dynamics of**  
 793  **$\delta_{\text{diluter}}$  measured (thick red line) and simulated (thin grey lines, one line per root system group, following a "swarm" pattern).**  
 794 **(b) Boxplot of simulated  $\delta_{\text{diluter}}$  values for each root system maximum depth, by 1 cm increment. (c) Temporal dynamics of**  
 795  **$\psi_{\text{leaf}}$  measured (thick green line) and simulated (thin grey lines, one line per root system group, following a "rollercoaster"**  
 796 **pattern). (d) Boxplot of simulated  $\psi_{\text{leaf}}$  values for each root system maximum depth, by 1 cm increment.**



797

798

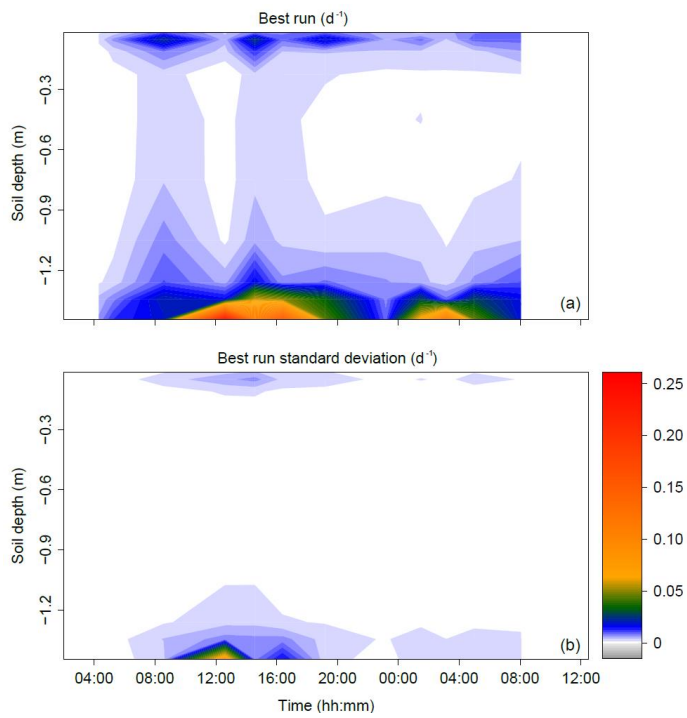
799

800

**Figure 6. Time series of the profiles of root water uptake per unit soil volume (sink term,  $d^{-1}$ ) computed with the physically-based model. (a) Sum of sink terms across the 60 groups of the population. (b) Variability of sink terms within the 60 groups of the population (1 standard deviation).**

801

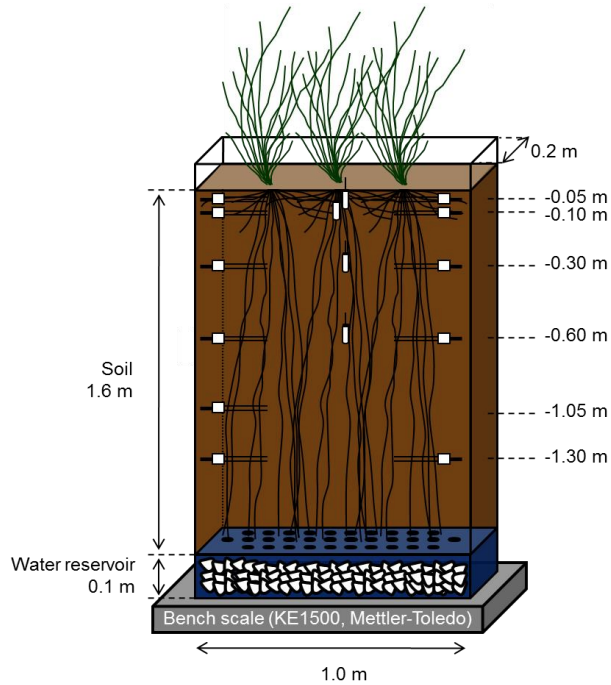


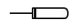
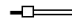


802

803 **Figure 7. Time series of the profiles of root water uptake per unit soil volume (sink term,  $d^{-1}$ ) computed with the statistical**  
 804 **model SIAR (a). Panel (b) reports the variance of the estimated sink term (1 standard deviation).**

805



-  Tensiometer (SMS 2000, SDEC)
-  Soil volumetric water content reflectrometers (CS616, Campbell Sci.)

807

808 Appendix A. Soil macro-rhizotron experimental setup with tall fescue cover

809  
810

$\theta_{\text{sat}}$ ( $\text{m}^3 \text{m}^{-3}$ )	$\theta_{\text{res}}$ ( $\text{m}^3 \text{m}^{-3}$ )	$\alpha$ ( $\text{m}^{-1}$ )	$n$ (-)
0.4	0.044	0.0285	2.29

Formatted: Font: (Default) Arial

Formatted Table

Formatted: Font: (Default) Arial

Appendix B. Soil retention curve and parameters optimized values [van Genuchten, 1980 - Burdine] [Meunier et al., 2017a]

811 **Appendix C. Timeline of destructive sampling**

DAS 166		DAS 167																								
		'night' data							'day' data													'night' data'				
Time	15:45	03:55	04:10	04:50	05:15	06:00	07:00	08:10	09:05	10:10	11:00	12:00	12:40	13:10	13:55	14:35	15:15	15:50	16:15	17:00	17:50	20:30	21:30	22:30	23:30	
Soil	x						x													x						
Leaves		x	x	x	x	x	x	x	x	x	x	x	x	x	x	x	x	x	x	x	x	x	x	x	x	x
roots	x																									
DAS 168		'night' data'											'day' data													
Time	00:00	00:30	01:00	01:30	02:00	02:30	03:00	04:00	04:30	05:00	05:30	06:00	07:00	08:00	08:30	09:00	10:00									
Soil										x																
Leaves	x	x	x	x	x	x	x	x	x		x	x	x	x	x	x	x									

Formatted: For  
 Formatted Tab  
 Formatted: For  
 Formatted: For  
 Formatted: For  
 Formatted: For  
 Formatted: For  
 Formatted: For  
 Formatted: For  
 Formatted: For

812

813 **Appendix D. Inverse modeling scheme**

814 The parametrization method was inverse modeling, with four targets: (i) minimizing the differences between observed  
815 and predicted  $\delta_{\text{tiller}}$  in each pool  $p$ , (ii) minimizing the difference between the standard deviations of observed and  
816 predicted  $\delta_{\text{tiller}}$  (temporal and population deviations altogether), (iii) minimizing the differences between observed and  
817 predicted  $\psi_{\text{leaf}}$  in each root system group  $i$ , (iv) minimizing the difference between the standard deviations of observed  
818 and predicted  $\delta_{\text{tiller}}$  (temporal and population deviations altogether). These targets translated as an objective function  
819 ( $OF$ ) to be minimized, where differences were normalized by the standard deviation ( $SD$ ) of observations in order to  
820 make the error function dimensionless:

821  $OF$

$$822 = \sqrt{\frac{1}{2} \left( \frac{1}{N_p N_t} \sum_i \sum_t \left( \frac{\delta_{\text{tiller},\text{obs}}(t) - \delta_{\text{tiller},p,\text{sim}}(t)}{SD(\delta_{\text{tiller},\text{obs}}(t))} \right)^2 + \frac{1}{N_i N_t} \sum_i \sum_t \left( \frac{\psi_{\text{leaf},\text{obs}}(t) - \psi_{\text{leaf},i,\text{sim}}(t)}{SD(\psi_{\text{leaf},\text{obs}}(t))} \right)^2 \right)}$$

$$823 + \left| \frac{SD(\delta_{\text{tiller},\text{obs}}(t)) - SD(\delta_{\text{tiller},p,\text{sim}}(t))}{SD(\delta_{\text{tiller},\text{obs}}(t))} \right| + \left| \frac{SD(\psi_{\text{leaf},\text{obs}}(t)) - SD(\psi_{\text{leaf},i,\text{sim}}(t))}{SD(\psi_{\text{leaf},\text{obs}}(t))} \right| \quad (D1)$$

824 where  $N_p$  is the number of  $\delta_{\text{tiller}}$  pools simulated (100) at each observation time,  $N_i$  is the number of plant groups  
825 simulated (60), and  $N_t$  the total number of observation times (40).

826 The global optimizer Multistart heuristic algorithm OQNLP (Optimal Methods Inc.) of the MATLAB (The  
827 MathWorks, Inc., USA) optimization toolbox was used to minimize the error function within the lower and upper  
828 limits of the parametric space reported in Table 1.

829 **Appendix E. Statistical determination of relative RWU profiles with SIAR**

830 The Bayesian inference statistical model SIAR [Parnell et al., 2013] was used to determine the profiles of relative  
831 contributions to RWU (rRWU, dimensionless) of ten identified potential water sources. These water sources were  
832 defined to originate from the soil layers 0.00-0.03, 0.03-0.07, 0.07-0.15, 0.15-0.30, 0.30-0.60, 0.60-0.90, 0.90-1.20,  
833 1.20-1.32, 1.32-1.37, and 1.37-1.44 m. Their corresponding isotopic compositions were obtained from the measured  
834 soil water isotopic compositions ( $\delta_{soil}$ ) and volumetric content ( $\theta$ ) values following Eq. (E1) [Rothfuss and Javaux,  
835 2017]:

836 
$$\delta_{soil,J} = \frac{\sum_{j \in J} \delta_{soil,j} \theta_j \Delta Z_j}{\sum_{j \in J} \theta_j \Delta Z_j} \quad (E1)$$

837 where J is the soil layer index, j is the soil sub-layer index, and  $\Delta Z_j$  is the thickness of the soil sub-layer j. Therefore,  
838 equation (E1) translates the soil water isotopic composition measured across sub-layers j into representative isotopic  
839 compositions of the different sources (i.e., across layers J). The computed  $\delta_{soil,J}$  were compared to  $\delta_{iller}$  values. For this,  
840  $\delta_{iller}$  measurements were pooled in twelve groups corresponding to different time periods. These groups were defined  
841 to best reflect the apparent temporal dynamics of  $\delta_{iller}$ .

842 For each of the twelve time periods:

- 843 (i) the function *siarmcmcdirichletv4* of the SIAR R package ([https://cran.r-](https://cran.r-project.org/web/packages/siar/index.html)  
844 [project.org/web/packages/siar/index.html](https://cran.r-project.org/web/packages/siar/index.html)) was run 500,000 times with prescribed burnin and thinby  
845 equal to 50000 and 15, respectively. The output of the model (i.e., the *a posteriori* rRWU distribution  
846 across the ten soil water sources J) was obtained from a flat Dirichlet *a priori* rRWU distribution (i.e.,  
847  $rRWU_j=1/10$ );
- 848 (ii) the ‘best run’ (*br*, dimensionless) was selected from SIAR’s output. It was defined as the closest solution  
849 of relative contributions across sources from the set of most frequent values (*mfv*, dimensionless), i.e.,  
850 the relative contribution with the greatest probability of occurrence. The best run was identified as  
851 minimizing the objective function below, i.e., the RMSE (root mean square error) with respect to the set  
852 of *mfv*:

853 
$$OF = \sqrt{\frac{\sum_{j=1}^{10} (mf v_j - br_j)^2}{10}} \quad (E2)$$

854 (iii)  $br$  was then multiplied by transpiration rate (in  $\text{m d}^{-1}$ ) and divided by soil layer thicknesses ( $\Delta Z_j$ , in m)  
855 to obtain sink terms ( $S_j$ , i.e. root water uptake rate per unit soil volume, expressed in  $\text{d}^{-1}$ ). The interest  
856 of sink terms in a comparison is that they do not vary with soil vertical discretization.

857 Steps (i)-(iii) were repeated a 1,000 times to estimate the variance of the best run for each time period and soil water  
858 source J.